

---

# The Mechanics of Recombination Disentangled by Dual Molecule Measurements

Master Thesis,\* from May 1, 2010 to April 30, 2011



Ludovit Pavel Zweifel

Nanoscience Curriculum

Faculty of Natural Science

University of Basel

Switzerland

---

\*Performed in the group of Prof. Dr. Cees Dekker at the Department of Bionanoscience, Kavli Institute of Nanotechnology, TU Delft, Netherlands

*Dedicated to my mother, Esther Zweifel Aellig*

# Contents

<b>1. Abstract</b>	<b>1</b>
<b>2. Introduction</b>	<b>2</b>
2.1. DNA Damages and Repair Mechanisms	2
2.2. Recombinational repair in <i>E. Coli</i>	2
2.3. The RecA Nucleoprotein Filament	3
2.4. The Challenge of Homology Search	5
<b>3. Material and Methods</b>	<b>6</b>
3.1. Experimental Set Up	7
3.1.1. Optical Tweezers (OT)	7
3.1.2. Magnetic Tweezers (MT)	8
3.1.3. Multichannel Flowcell	10
3.1.4. Bead Tracking	11
3.2. Experimental Assay	12
3.2.1. Getting Started	13
3.2.2. The Fishing Procedure	13
3.2.3. Tethering of Magnetic Beads	14
3.2.4. Assay 1	15
3.2.5. Assay 2	15
3.2.6. Assay 3 and Assay 5	15
3.2.7. Assay 4	16
3.3. Biophysical Characterization of the Constructs	17
3.3.1. Characterization of the Optical Constructs	17
3.3.2. Characterization of the Magnetic Constructs	19
3.3.3. RecA Nucleoprotein Filament Formation	20
3.4. Dual-Molecule Experiments	22
3.4.1. Push-Probe Experiments for Force Spectroscopy	22
3.4.2. Sliding Experiments for Friction Tribology	23
<b>4. Results</b>	<b>25</b>
4.1. Results: Assay 1	25
4.2. Results: Assay 2	28
4.3. Results: Assay 3	30
4.4. Results: Assay 4	31
4.5. Results: Assay 5	33
<b>5. Discussion</b>	<b>35</b>
5.1. Interpretation of the results	35
5.2. A model for homology recognition	39
5.3. The speed of recognition	41
<b>6. Conclusions</b>	<b>43</b>
<b>7. Acknowledgement</b>	<b>44</b>
<b>A. Appendix</b>	<b>48</b>

## Contents

<b>B. Appendix</b>	<b>49</b>
<b>C. Appendix</b>	<b>52</b>
<b>D. Appendix</b>	<b>56</b>

## 1. Abstract

Homologous recombination (HR), the exchange of homologous sequences of deoxyribose nucleic acid (DNA), is a process found in all kingdoms of life. In this work we investigate the mechanism of recognition of homology (complementary DNA) during bacterial DNA double-strand (ds) break repair with a biophysical approach. In *Escherichia coli* (*E. coli*) the fast and accurate search for homologous sequences is mediated by the Recombinase A (RecA) protein. RecA is a member of a family of ATPase proteins with two independent DNA binding sites and serves as an archetype for this class of homologous DNA repair proteins. The 38kD RecA monomers assemble on single-stranded (ss) DNA and form a nucleoprotein filament (NPF) via their primary DNA binding site (PBS), and they search homologous sequences in intact dsDNA via their secondary DNA binding site (SBS). With a unique combination of magnetic tweezers and dual-bead optical tweezers, we were able to manipulate single RecA-NPFs and single DNA molecules simultaneously. This allowed us to probe the mechanics of homology recognition by establishing a single point of contact between these molecules. We find that the interactions between the SBS of a RecA-NPF with intact dsDNA are very weak. Our results indicate that, in contrast to the common doctrine, the RecA-NPF does not actively destabilize the donor duplex, but that the first step in the recognition process is the spontaneous formation of a bubble of ssDNA (dsDNA breathing). Stable joints were exclusively formed when both strands of the donor duplex bind to one of the two independent binding sites in the RecA-NPF. By investigating the interactions between RecA-NPFs and heterologous dsDNA we show that nonspecific binding of bubbles is at least two orders of magnitudes weaker than homologous interactions. In line with the picture of spontaneous breathing of dsDNA, we find that the speed and strength of homologous pairing are strongly enhanced by negative torsional stress. Furthermore we provide evidence that homology recognition can take place at any intermolecular contact point. On the basis of our findings, we propose a model in which the fidelity of the recognition process is defined by the distance between the PBS and SBS of a RecA-NPF and their individual binding affinities to ssDNA.

## 2. Introduction

### 2.1. DNA Damages and Repair Mechanisms

From the identification of DNA as the blueprint of life it is obvious that maintaining its stability is crucial for a coherent genetic code. Mutations in genes critical for the regulation of the cell growth, for instance, can lead to carcinogenesis [1]. Although DNA is extremely stable, endogenous failures in cell processes as well as exogenous agents can inflict various types of damage [1, 2]. Estimates of the number of DNA-damage events in a single human cell range from  $10^4$ - $10^6$  per day [3]. Cells react with different responses to these damages depending on their severity, ranging from apoptosis [4] to DNA repair [1, 2]. Throughout evolution prokaryotic and eukaryotic cells have developed different strategies to repair differently damaged DNA. Most harmful among DNA defects are double-strand breaks (DSB) induced by ionizing radiation, radiomimetic drugs and oxygen radical species (exogenous) [5] or when replication forks encounter obstacles or single-strand interruptions (endogenous) [6]. DSBs can interrupt the coding sequences of a gene, alter chromosome organization and perturb the systems that ensure correct DNA replication, chromosome packaging and chromosome segregation [6].

Cells have adopted two mechanisms for the repair of DSBs: non homologous end-joining (NHEJ) and homologous recombination (HR). NHEJ is a pathway by which two DNA ends are ligated at regions of little or no homology, which can lead to loss of information from the DNA because of resection of the broken ends [7]. HR is a more reliable, error-free repair mechanism which is highly conserved between organisms from all kingdoms of life [8]. In contrast to NHEJ, HR can also cope with free ends, when one end of a DSB is lacking [6]. The broken DNA molecule forms a synapsis with another undamaged DNA duplex of homologous sequence, after which a combination of DNA synthesis and processing restores the broken molecule. The main reaction during homologous recombination is the strand exchange between two homologous DNA molecules. Search, recognition and exchange of complementary partners are driven by the RecombinaseA (RecA) superfamily of ATPase conserved from bacteria to humans [6, 8]. The conservation of structure and function throughout this family of recombinases allows the use of *E. Coli* RecA as a model for HR in humans [8, 9].

### 2.2. Recombinational repair in *E. Coli*

Three fundamental stages can be identified in the process of homologous recombination [6, 8] (fig.1). A presynaptical stage, where the DSB are prepared for the invasion into a intact dsDNA (fig.1a-c). The blunt duplex end of the DSB is converted into a 3' single-strand overhang by resection of the 5'-end. In *E. Coli* the protein complex responsible for this step is the RecBCD enzyme [10]. After the resection of the 5' end single-strand, RecA assembles on the left over 3' overhang forming a helical nucleoprotein filament (NPF) [10, 11, 12]. The RecA-NPF catalyses the search and recognition of homologous counterparts. The formation of a synapsis between the broken end and an intact DNA duplex (D-loop) upon encounter of a complementary sequence is the second stage common to HR (fig.1d,e) [8, 10]. During the postsynaptic stage the D-loop can either be converted to a Holliday junction (HJ) or disintegrated by releasing the invading RecA-NPF. In *E. Coli*, RecG is thought to be responsible for the conversion of the D-loop into a HJ (fig.1f) [15] and RuvABC proteins for the branch migration and cleavage of the HJ (fig.1g,f) [16]. Finally nicks are repaired by DNA ligase revealing two separated DNA duplexes [10].

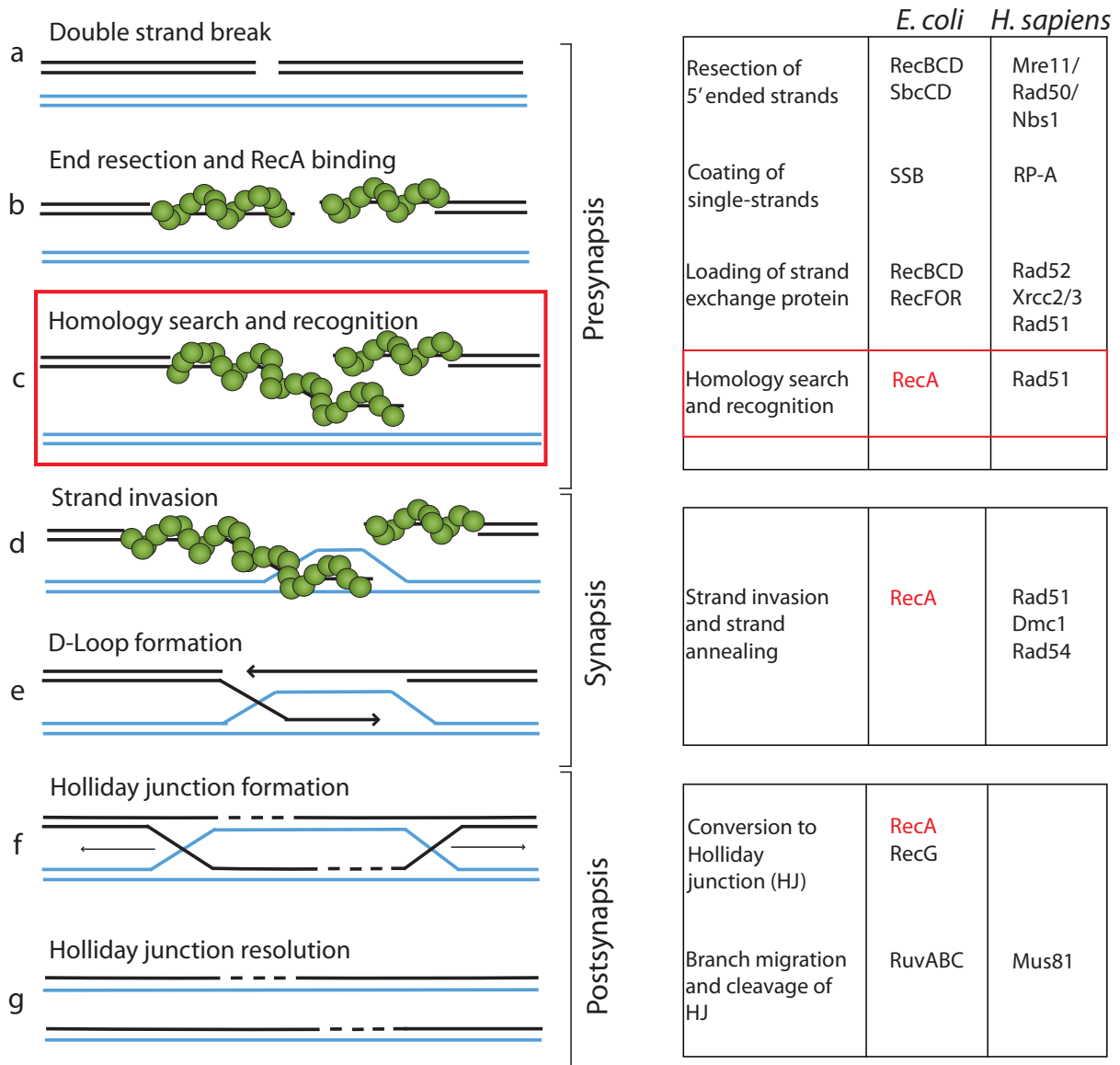


Figure 1: Recombinational repair in *E. Coli*. **a**, a double-strand break occurs, is detected and the blunt duplex end converted in a 3' single-strand overhang [10]. **b**, RecA assembles on the left over 3' overhang forming a helical nucleoprotein filament (NPF) [10, 11, 12]. **c**, the RecA-NPF catalyses the search and recognition of homologous counterparts. **d** and **e**, strand invasion and formation of a synapsis between the broken end and an intact DNA duplex (D-loop) upon encounter of a complementary sequence [8, 10]. **f**, the D-loop can either be converted to a Holliday junction (HJ) (**g**) or disintegrated by releasing the invading RecA-NPF (not shown).

### 2.3. The RecA Nucleoprotein Filament

The central reaction in HR is the strand exchange between two homologous DNA molecules governed by a RecA-NPF. RecA has a primary (PBS) and a secondary (SBS) binding site. Assembly on single-stranded (ss) DNA overhang is performed via the PBS (ssDNA·RecA). The 38kD RecA monomers bind to ssDNA forming a helical NPF with 6.2 RecA proteins per turn and three nucleotides per RecA monomer [8, 12]. The NPF formation is highly cooperative, and its nucleation requires the binding of five to six protomers [12]. No ATP hydrolysis is needed for the NPF assembly [11]. In this work, a non-hydrolysable ATP analogue (ATP- $\gamma$ -s) is used as a cofactor for nucleoprotein filament formation. The ssDNA in the PBS is in a highly deformed conformation, stretched and underwound with 18.5 nucleotides per turn and an average rise of 5.1Å per

## 2. Introduction

nucleotide [11]. However, the spacing between single nucleotides is non-equidistant. The repeating unit of the ssDNA is a group of three nucleotides locally arranged in a B-DNA-like conformation with an axial rise of  $4.2\text{\AA}$  [12]. The B-DNA-like conformation within the nucleotide triplet is compensated by a  $7.8\text{\AA}$  axial rise and a left-handed twist of  $-42^\circ$  from the last base of one triplet to the first of the next [12]. Filaments can also form on dsDNA [13], in which case a similar conformation as for ssDNA is observed [12].

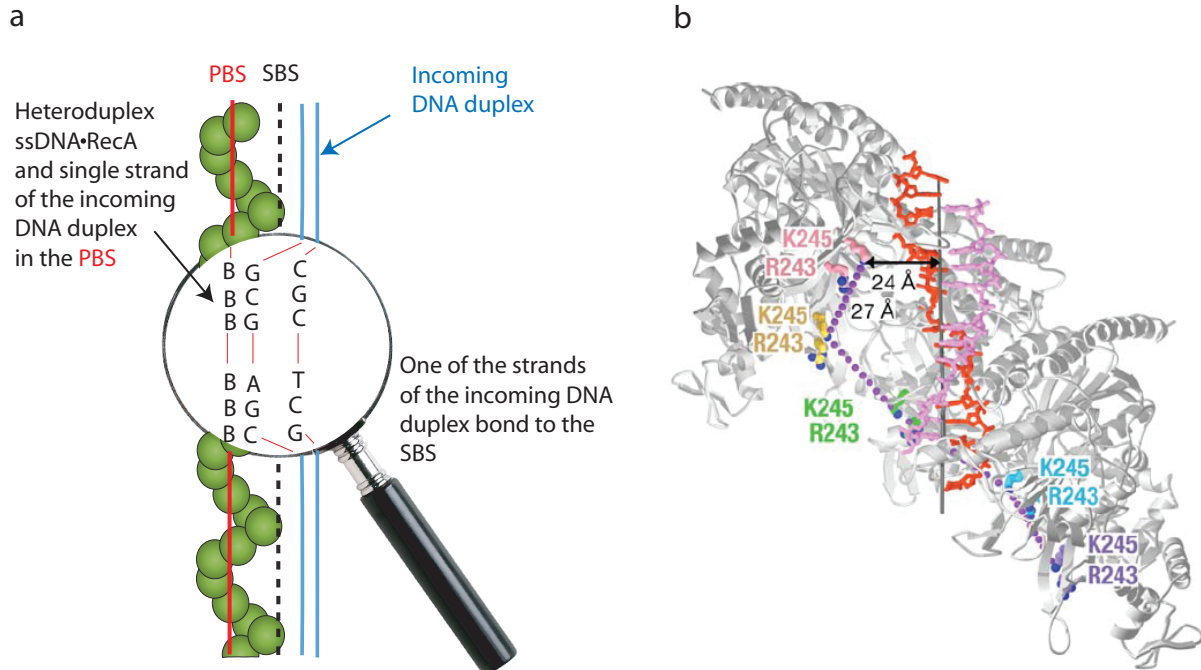


Figure 2: Structure of a RecA-NPF. **a**, schematic drawing of a RecA-NPF formed on a ssDNA interacting with either homologous or heterologous dsDNA bound to the SBS. **b**, Resolved structure of a RecA filament formed on ssDNA according to [12]. The distance between the PBS and the SBS ( $24\text{\AA}$ - $27\text{\AA}$ ) is indicated by an arrow.

Prior to the exchange the RecA-NPF locates a complementary DNA duplex without ATP hydrolysis [14]. Incoming intact dsDNA during homology search binds in first instance to the NPF via the SBS (RecA-dsDNA). The local B-DNA-like structure of the nucleotide triplet unit of ssDNA in the PBS restricts the search of homology in the SBS bound dsDNA to Watson-Crick-type base pairing. A distance of  $24\text{\AA}$ - $27\text{\AA}$  was found between the RecA-NPF axis and dsDNA bound to the SBS (ssDNA·RecA-dsDNA) [12].

## 2.4. The Challenge of Homology Search

The speed and fidelity of the search for homology by RecA pose a challenge from a mechanistic and thermodynamic point of view. RecA-NPF's can detect very weak signals (short homologous sequences) in a large heterologous background. It was demonstrated that the addition of 200'000 fold heterologous dsDNA does not affect the efficiency of the joint molecule formation *in vivo* [18]. Furthermore, the search of homology in a large excess of heterologous sequences has to be successful within a cell's life cycle, implying a sampling frequency of  $10^3$ - $10^4$ s<sup>-1</sup> [19]. How the mechanism works which allows the RecA-NPF to conduct the search for homology with such a speed while maintaining high-fidelity remains a matter of debate. In this work we shed light on the mechanism of search and recognition with a biophysical approach by establishing single points of contact between RecA-NPF and DNA. We used a dual molecule assay to adress the following questions:

- **What happens at the point of contact?**
- **Which mechanism allows fast search without energy consumption (no ATP hydrolysis required)?**
- **What provides the fidelity of the recognition process?**

### 3. Material and Methods

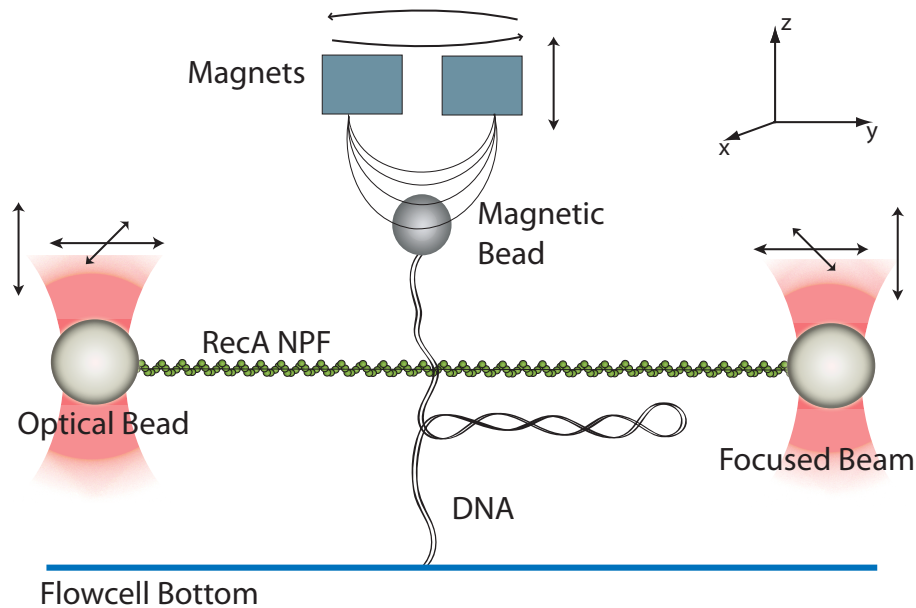


Figure 3: Example of a experimental assay. Two molecules are clamped by magnetic and dual-optical tweezers (sec.3.1 and app.A). A dsDNA molecule is clamped between a magnetic bead and the bottom of the flow cell. The magnetic tweezers show ideal force clamp characteristics and provide access to supercoils. A second molecule, a RecA-NPF, is tethered between two optical beads. The optical tweezers enable movement of the two optical beads in three-dimension. Interactions between the two molecules are probed by bringing the molecules into contact. Different assays have been established (fig.8) and various types of experiments have been performed (sec.3.4)

We have established a dual molecule assay by the combination of magnetic tweezers with dual-bead optical tweezers (fig.3) [20]. The assay enables individual control of two single molecules. The dual-bead optical tweezers offer accurate three-dimensional manipulation of a molecule tethered between two optically trapped beads. The magnetic tweezers can induce supercoils and act as a ideal force-clamp. In a magnetic tweezers configuration, molecules are at one end tethered to a trapped magnetic bead and on the other end to the flowcell. The three-dimensional flexibility of the optical traps allows to bring the optically and magnetically tweezed constructs into contact. In this way we performed different types of experiments on various biological constructs. The biophysical approach allows the measurement of the binding energies involved in the recognition process. By using the magnetic bead as a force probe, we performed force spectroscopy on single point contact between RecA-NPF and DNA. Furthermore, we realized tribology measurements by sliding bare as well as RecA covered DNAs across each other while destabilizing one of the molecules gradually.

### 3.1. Experimental Set Up

The main components of the setup are magnetic tweezers and dual-bead optical tweezers for trapping particles and a multichannel flowcell in which the experiments are done. All motors, beam steering with the acousto-optical deflectors (AOD's), flow speed through the flowcell, the output signals of the position sensitive detectors (PSD's) and video microscopy by a CMOS camera are controlled by a custom made LabView program. In the subsequent sections the general outline and major components of the setup are briefly explained. A detailed description can be found in J.F. den Blankens master thesis [20] and in the appendix A.

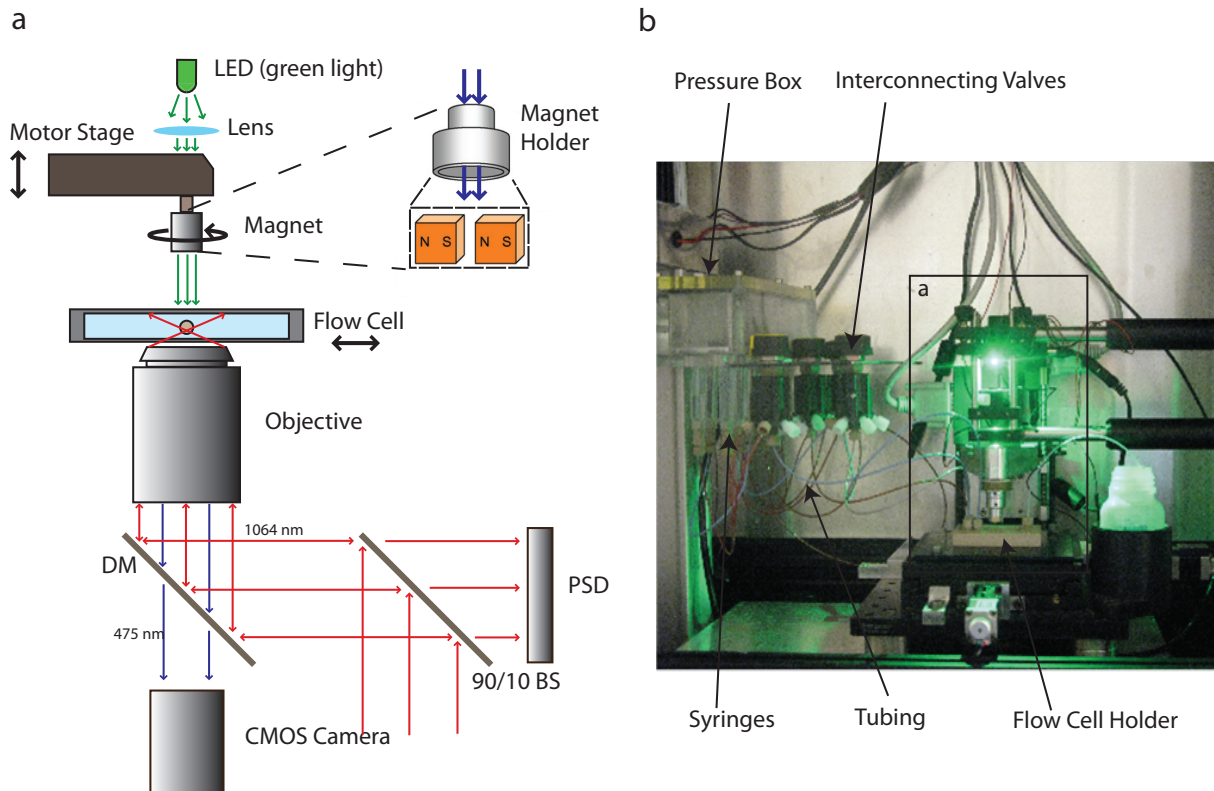


Figure 4: Experimental set up. **a**, schematics of the magnetic tweezers and parts of the optical tweezers (a detailed description of the optical path can be found in appendix A and in [20]). A green LED illuminates the flow cell through a hole in the magnet holder. The magnet holder contains two permanent magnets and is placed above the flow cell holder. The flow cell holder is fixed on a moveable stage and placed on top of the objective, which is used for focusing of the laser beams and collecting the scattered light of the beads in the flow cell. **b**, front view picture of the magnetic tweezers and flow system. A pressure box with ten syringes is connected to the four inlets of the flow cell holder via valves.

#### 3.1.1. Optical Tweezers (OT)

Dielectric, spherical beads can be trapped by focused laser beams if the gradient force pulling the particle towards the focal point overcomes the scattering force pushing it away from that region [21]. Therefore, the laser beam must be sharply focused by an objective with high numerical aperture (NA) to achieve a steep gradient in the light (fig.4a) [22]. If the radius  $r_{opt}$  of the dielectrical sphere is much larger than the wavelength  $\lambda$  of the trapping laser ( $r_{opt} \gg \lambda$ ) then the optical forces can be described by ray optics (Mie regime)[23]. If the  $r_{opt}$  of the dielectrical sphere is much smaller than the wavelength  $\lambda$  of the trapping laser ( $r_{opt} \ll \lambda$ ) then the optical forces can be calculated by treating the particle as a point dipole (Rayleigh regime) [23]. Here, we

### 3. Material and Methods

use a 4W, diode-pumped Nd:YAG laser system (Coherent Compass 1064-4000M) operating on TEM<sub>00</sub> mode, which creates a p-polarized Gaussian shaped laser beam of  $\lambda=1064\text{nm}$  (fig.4a). A combination of half-wave plates and polarizing beam-splitters is placed directly after the laser creating two separated beams and thus two individual traps. Each beam can be steered individually in x-, and y-direction with AODs, while the relative z position can be controlled by a moveable lens in one of the beam paths (see appendix A). This allows the user to freely manoeuvre the beads with respect to each other. Both beams are sharply focused by the same inverted water-immersion objective, enabling simultaneous changes of both traps in z-direction.

Since the dielectrical polystyrene beads (Sphero<sup>TM</sup>, Streptavidin Polystyrene), used throughout the experiments, have a radius  $r_{opt}$  of  $\sim 1\mu\text{m}$ , neither the conditions for the Mie nor for the Rayleigh regime are satisfied. In this intermediate regime electromagnetic forces can not be calculated analytically [24] and are thus determined experimentally [20]. For small displacements, the restoring force of the trap (in each dimension) on the bead  $F_{opt}$  is proportional to the offset from the equilibrium position  $x$ . In other words the trap acts like a Hookean spring, while the characteristic stiffness  $\kappa$  is proportional to the light intensity [20].

$$F_{opt} = -\kappa x \quad (1)$$

A calibration in lateral (xy-plane), and axial direction (z-axis) was performed in [20] and a maximum stiffness of  $\kappa=190\text{pN}/\mu\text{m}$  and  $\kappa=40\text{pN}/\mu\text{m}$  respectively obtained. Hereafter, we will refer to the dielectrical polystyrene beads as optical beads.

#### 3.1.2. Magnetic Tweezers (MT)

Superparamagnetic, spherical beads (Dynabeads<sup>®</sup> MyOne<sup>TM</sup>, Streptavidin C1) perceive a force by an inhomogenous magnetic field  $\mathbf{B}$ . A magnetic tweezers is simply realized by two permanent magnets closely spaced in a magnet holder placed above a flowcell (fig.4). The magnetic field in x-, and y-direction is homogenous on the scale of the radius of a superparamagnetic bead  $r_{mag}$  ( $\sim 0.5\mu\text{m}$ ). Thus the force acting on the superparamagnetic beads is exclusively directed in z-direction and depends on their relative magnetic permeability  $\mu_r$  and on the gradient of the magnetic field  $B_z$  exerted by the permanent magnets,

$$F_{mag} = \frac{2\pi r_{mag}^3}{\mu_0} \left( \frac{\mu_r - 1}{\mu_r + 2} \right) \frac{\delta B_z}{\delta z} \quad (2)$$

with  $r$  the radius of the bead and  $\mu_0$  the magnetic permeability in vacuum [26]. The height of the magnets in respect to the flowcell and thus the magnetic force acting on the bead is motor controlled (fig.4a and b). As for the optical traps, forces acting on a magnetic bead were determined experimentally. A tethered magnetic bead behaves like an inverted pendulum [25], whereat Brownian fluctuations determine the horizontal deflection ( $\Delta x$ ,  $\Delta y$ ) out of the equilibrium position. The analysis of the horizontal Brownian motion of the particle permits measurement of the stretching force. Using the equipartition theorem, the vertical magnetic force  $F_z$  can be evaluated through the simple formula

$$F_z = \frac{k_b T l}{\langle \delta x^2 \rangle} \quad (3)$$

where  $k_b$  is the Boltzmann constant,  $T$  the absolute temperature,  $l$  the end-to-end extension of the linking molecule and  $\langle \delta x^2 \rangle$  the variance of the lateral fluctuations (x- or y-direction)[25]. In this work, we used two different sets of magnets. The magnet height versus force curves used for the calibration of the force exerted on the superparamagnetic beads of  $r_{mag}$  ( $\sim 0.5\mu\text{m}$ ) are shown in figure 5.

Due to an anisotropy in their magnetic polarization  $\mathbf{M}$ , superparamagnetic beads have an easy axis of polarization which enables the application of a torque  $\Gamma$  to the beads

### 3. Material and Methods

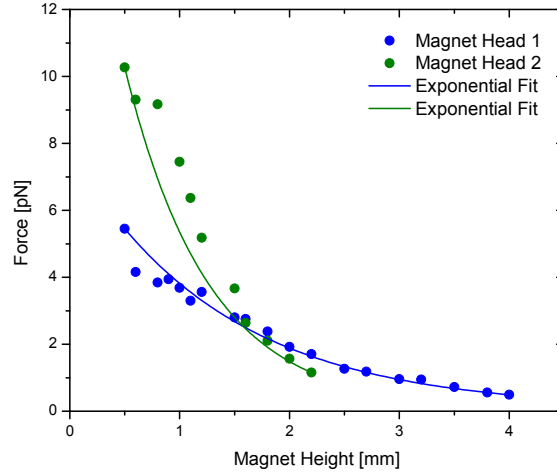


Figure 5: Magnet height versus force curves. Two different sets of permanent magnets were applied in this work. The exponential fits ( $F_{\text{Mag. Head 2}} = (6.8382 \pm 0.26) \exp[(-0.62574 \pm 0.0312) \cdot l]$ ,  $F_{\text{Mag. Head 1}} = (17.451 \pm 1.01) \exp[(-0.93312 \pm 0.0657) \cdot l]$ ) are used to determine the force exerted on a superparamagnetic beads of  $r_{\text{mag}} (\sim 0.5 \mu\text{m})$  used throughout this work

$$\Gamma = \mathbf{M} \times \mathbf{B} \quad (4)$$

A second motor controls the rotation of the magnet holder and enables twisting and coiling of dsDNA (fig. 4 and fig. 3). This is possible because the torque induced by the tethered molecule or by thermal fluctuations is orders of magnitudes smaller than magnetically induced torque. A tethered superparamagnetic bead shows ideal force-clamp characteristics and serves as a highly sensitive force-probe, with a resolution set by thermal fluctuations ( $10 \text{ fN} / \sqrt{\text{Hz}}$ ). As from now we will be refer to superparamagnetic beads as magnetic beads.

### 3. Material and Methods

#### 3.1.3. Multichannel Flowcell

The dual molecule experiments were performed in multi-channel flow cells [17]. The flow cells used in this work have four channels with individual inlets and a common outlet (fig.6). Fluids flushed into single inlets remain partitioned in the main channel due to the laminar character of the flow. Hence, these multi-channel flow cells enable flushing in and switching between different types of substrates (buffers, DNA and beads) while maintaining spatial separation. The four inlets are connected to a pressure box with ten syringes addressable with interjacent valves, enabling fast substrate exchange (fig.4b). An over pressure of up to 1.8bar in the pressure box pushes the substrates through the flow. In the four channels, different flow speeds can be generated by choice of the diameter of the interconnecting tubings between syringes, valves and inlets (fig.4b). The multichannel laminar flowsystem is fundamental to perform our experiments that depend on the assembly of optical and magnetic constructs which require different buffer conditions at the same time. The build-up of the different constructs used throughout this work will be explained in the sections 3.2.4 to 3.2.7.

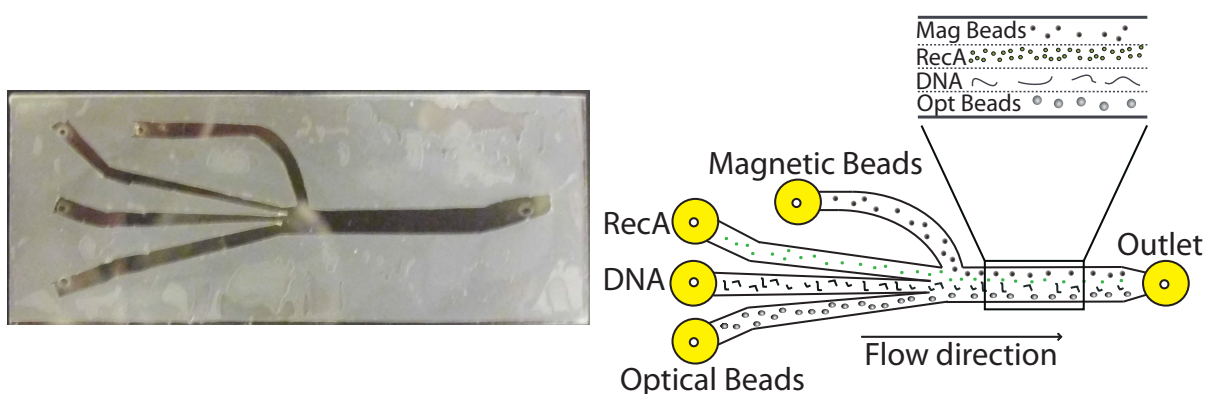


Figure 6: Picture and schematic sample configuration of the flow cell. Four channels are addressable by individual inlets. Fluids in the main channel remain separated due to the laminar character of the flow. Zoom-in of the main channel will be used throughout this work to emphasize the different flow cell configuration

The flow cell is constituted by two glass slides and parafilm. Four holes for the inlets and one hole for the outlet are drilled in one of the glass slides by a sandblaster and afterwards both slides are sonicated in ethanol. Subsequently the second glass slide is being coated on one side with nitro cellulose (see app.B). The pattern of the flow cell is cut out from the parafilm prior to its deposition on the coated glass slide. The glass slide with the holes is put on top and the whole sandwich structure sealed by heating up to 90°C. Finally the flow cell is mounted in a custom made holder which enables the connection between inlets and valves.

## 3.1.4. Bead Tracking

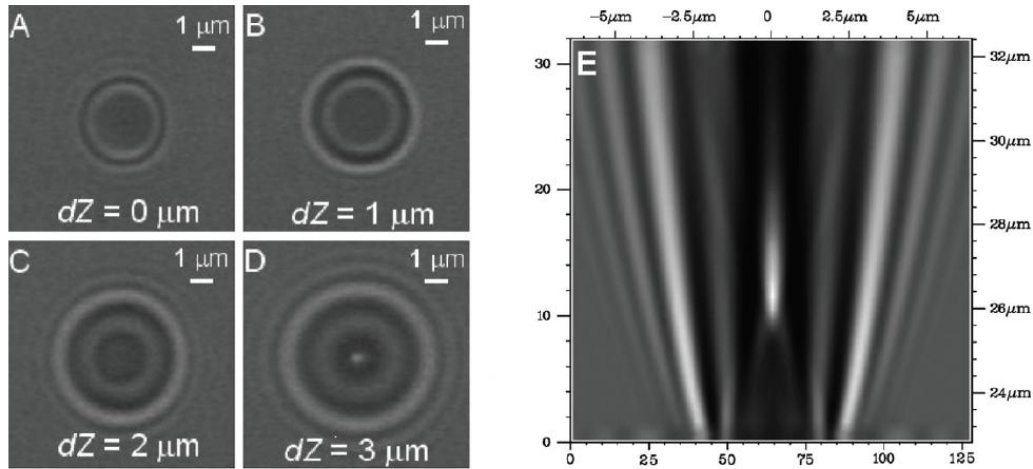


Figure 7: Interference pattern of a bead at different heights. **a-d**, different ring pattern correspond to different z-position. Detection of the z-position of the beads by the CMOS camera is based on this principle. **e**, image of a look-up table (LUT). The cross-section of the interference pattern is plotted for increasing z-position. A calibration is achieved by focussing on a bead which sticks on the flow cell bottom, and subsequently defocussing with known step size (moving the objective by a piezo stage). Figures taken from [20]

The flow cell is illuminated through a small hole in the magnet holder by a green light emitting diode (LED) which is placed above the holder. The tracking of the position of multiple beads (for both, magnetic and optical) is based on the interference pattern created by the LED light and scattered light of the beads. The objective which focuses the laser beams also collects the light (see 3.1.1) which is transmitted to a CMOS camera (Falcon 1.4M100, Dalsa, 100Hz) via a dichroic mirror. Since the beads are spherical the interference pattern on the camera is coaxial and distributed depending on the distance of the beads to the focal plane of the objective (fig.7a-d). A centre-of-mass autocorrelation of the camera image allows for video microscopy with a resolution of  $(3,8\text{\AA}/\sqrt{Hz})$ .

### 3.2. Experimental Assay

Different types of dual molecule experiments have been performed with different types of constructs. RecA-NPFs have been assembled on ds- and ssDNA tethered between two optical beads (optical construct) or between the bottom of the flow cell and a magnetic bead (magnetic construct). These constructs were brought into contact with dsDNA and ssDNA leading to eight possible geometrical configurations. By the use of either heterologous or homologous DNA the number of possible assays is doubled (tab.1). We performed experiments on five different assays shown in figure 8.

Table 1: Possible RecA NPF-DNA dual-molecule experiments with either homologous or heterologous constructs. The geometrical configurations used in this work (fig.8) are highlighted

	Magnetic Construct	Optical Construct	Magnetic Construct	Optical Construct
Hetero	dsDNA · RecA	dsDNA	dsDNA	dsDNA · RecA
	dsDNA · RecA	ssDNA	ssDNA	dsDNA · RecA
	ssDNA · RecA	dsDNA	dsDNA	ssDNA · RecA
	ssDNA · RecA	ssDNA	ssDNA	ssDNA · RecA
Homo	dsDNA · RecA	dsDNA	dsDNA	dsDNA · RecA
	dsDNA · RecA	ssDNA	ssDNA	dsDNA · RecA
	ssDNA · RecA	dsDNA	dsDNA	ssDNA · RecA
	ssDNA · RecA	ssDNA	ssDNA	ssDNA · RecA

In the subsequent section the formation of the different constructs in the flow cell is described. After a short explanation of the steps common to the preparation of all experimental assays, specific details in the construction of individual assays shown in figure 8 will be examined. More specific protocols describing the preparation methods can be found in appendix B.

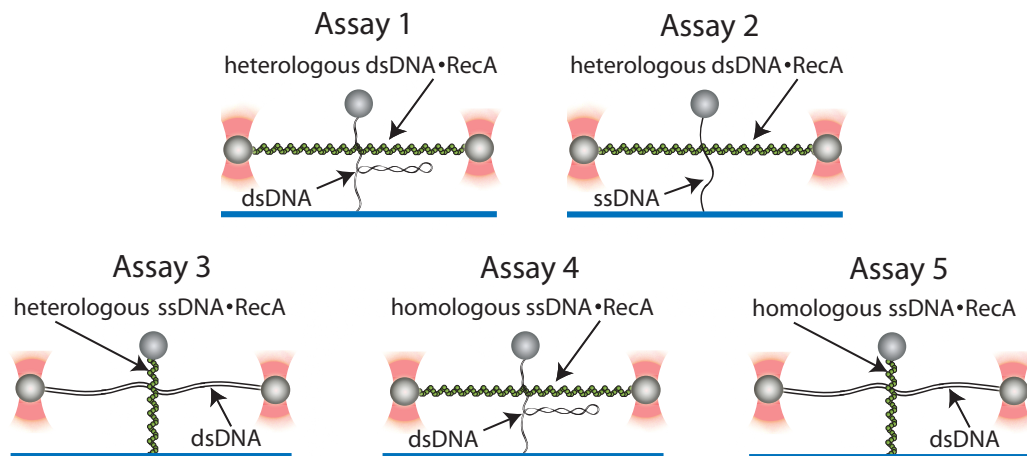


Figure 8: All experimental assays formed within this work at a glance. RecA-NPF were formed on ds- and ssDNA tweezed by magnetic or optical traps.

### 3.2.1. Getting Started

Prior to experiments the multichannel flow cell is incubated with a solution of anti-Dioxigenin (anti-DIG) which preferentially binds to the bottom glass slide coated with nitro cellulose. Anti-DIG is subsequently flushed out with and replaced by Bovine serum albumin (BSA). BSA is incubated before attaching the flow cell to the rest of the flowsystem to reduce non-specific binding between beads and flow cell. Flow cells can be reused, but have to be stored filled with  $\text{NaNO}_3$  containing buffer to prevent bacterial growth and reincubated with BSA before experiments.

Optical constructs, the conjunction between optical beads and DNA, are realized by streptavidin-biotin bonds. The beads are coated with streptavidin, enabling the attachment of biotinylated DNA ends. The optical beads are washed in a high salt buffer to extract dissolved streptavidin from the solution prior to being flushed in. This procedure increases the binding efficiency between DNA and beads, since less biotin handles on the DNA are occupied by free streptavidin.

Magnetic constructs are formed between the passivated, anti-DIG covered bottom of the flow cell and streptavidin coated magnetic beads. Therefore DNA used to build magnetic constructs is biotinylated on one end and has a DIG label on the other. As with optical beads, magnetic beads have to be washed before use which is done in a low salt Tris buffer (TE).

### 3.2.2. The Fishing Procedure

The optical beads do not require any further preparation after washing. Optical constructs are formed by “fishing” (fig.9). Two optical beads are trapped in the optical bead channel and subsequently moved to the adjacent DNA containing channel (fig.9a). One of the beads (bead 1) iteratively approaches and recedes from the other bead (bead 2) which is held fixed upstream to bead 1 (fig.9b-9e). Eventually DNA flowing by binds with one of its biotinylated ends to the streptavidin coated bead 1 (fig.9c). By approaching, the other end of the flow-stretched DNA can bind to the streptavidin coated bead 2 (fig.9c and d).

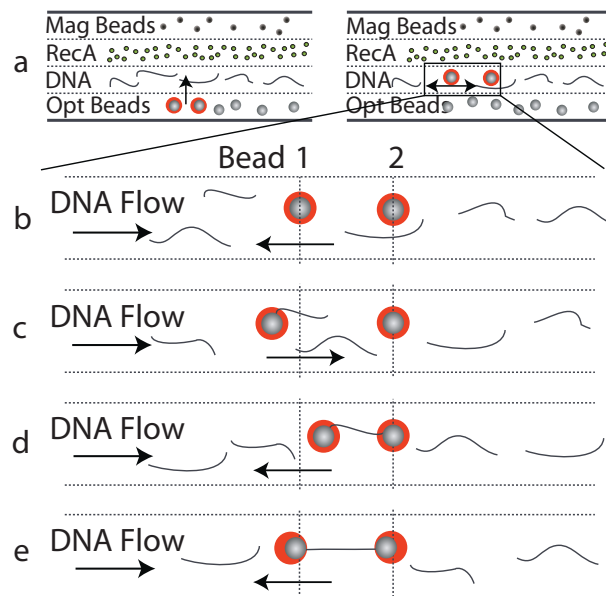


Figure 9: The fishing procedure. **a**, catching and aligning of two optical beads. **b**, forth and back movement of bead 1. **c**, attachment of DNA to bead 1. **d**, binding of the other DNA end to bead 2. **e**, detection of a tethered DNA molecule (bead 2 acts as a force probe by tracking its displacement from the center of the trap (equilibrium position))

### 3. Material and Methods

Successful catching of a single DNA molecule between the two optical beads can be detected by a displacement of bead 2 from the center of the optical trap (fig.9d). This procedure where bead 1 fishes for DNA and bead 2 acts as a force-probe is called “fishing”. It can be distinguished between single and multiple DNA tethers between the beads by the characteristic force-response of single DNA molecules upon stretching. Optical bead catching and the fishing procedure have been automated to increase the general throughput of the experiments.

#### 3.2.3. Tethering of Magnetic Beads

In contrast to the optical beads, magnetic beads are incubated with DNA before being flushed into the flow cell. The distribution of bound DNA to the magnetic bead has to be fairly sparse to allow attachment of a magnetic bead to the flow cell bottom by a single DNA molecule. Hence, incubation prior to the experiments is done with a low concentration of DNA in TE-buffer. The DNA binds to streptavidin on the bead surface with the biotin labels at one of its ends, leaving the DIG label on the other end accessible. The magnetic beads are ready to be flushed into the designated channel of the flow cell (fig.6) after passivation of the left-over, non-DNA occupied streptavidin on the bead surface with biotinylated BSA (bio-BSA). Passivation should avoid unwanted binding of DNA attached to the optical beads, since formation of the optical construct is also provided by streptavidin-biotin bonds. The flow speed is adjusted such that the beads are able to settle in the channel and eventually undergo specific binding to the bottom via antiDIG-DIG bonds. Subsequently, non-sticking and non-specifically attached beads are flushed out of the channel by TE-buffer. Remaining unbound magnetic beads attached to the bottom of the flow cell act as reference for height measurements between the bottom of the flow cell and magnetic constructs (fig.10).

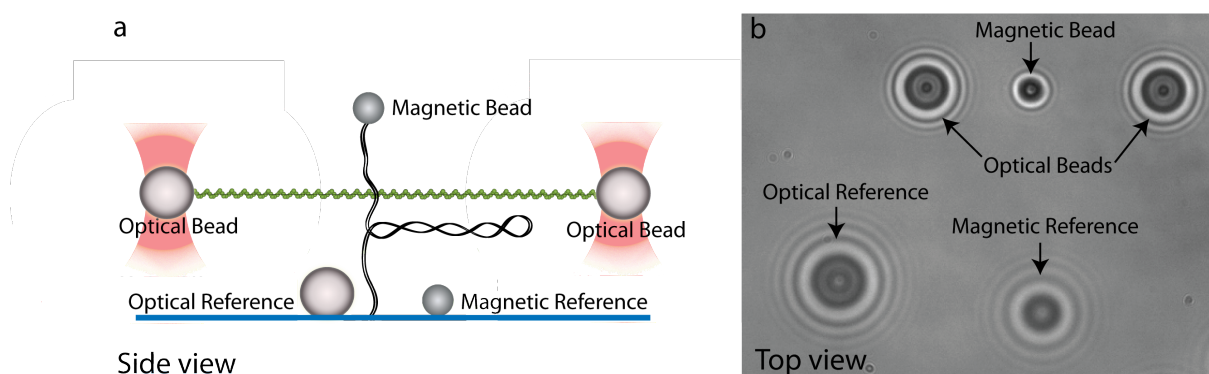


Figure 10: Example geometry after assay formation. **a**, schematics of the configuration after the assembly of the constructs. The magnetic and optical constructs are brought into contact at a single point. Magnetic and optical beads are placed on the bottom of the flow cell and act as height reference for the tweezed constructs. **b**, top view picture of the bead configuration during an experiment

The confinement of the channels due to laminar flow assures that the magnetic constructs are formed at the designated locations (fig.6). The external magnets are dismantled during flush in to avoid aggregation of the magnetic beads at the top of the flow cell which occludes the field of view.

### 3. Material and Methods

#### 3.2.4. Assay 1

The purpose of the assay described in this section is to probe interactions between RecA-NPFs formed on dsDNA (48kb) and heterologous, coilable dsDNA (10kb) ((OT)dsDNA·RecA-heterologous dsDNA(MT)). The RecA-NPF is tethered between the optical beads, while the magnetic tweezer is used to induce negative or positive supercoils into the dsDNA as shown in figure 8.

The configuration of the flow cell during the formation of this assay can be reconstructed with help of figure 11. In the beginning optical beads, dsDNA (48kb) in TE<sup>+</sup>-buffer, only TE<sup>+</sup>-buffer and prepared magnetic beads are flushed in (fig.11 step 1). Subsequently, coilable magnetic constructs attached by single dsDNA molecules are searched and characterized. Distinction between single or multiple, coilable or non-coilable dsDNA is made by analyzing the coiling behaviour (fig.14a). After locating of appropriate magnetic constructs, optical beads are placed in their vicinity on the bottom of the flow cell (fig.11 step 2). These act as height reference for the optical beads (fig.10).

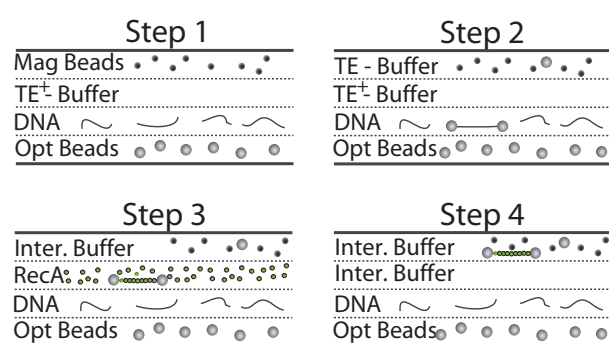


Figure 11: Build up of assays with the RecA-NPF tweezed between the optical traps

RecA-NPF is maneuvered in proximity of the magnetic construct in the magnetic bead channel subsequent to the successful formation (fig.11 step 4 and fig.10).

#### 3.2.5. Assay 2

Instead of a 10kb heterologous dsDNA, in assay 2 ((OT)dsDNA·RecA-heterologous ssDNA(MT)) a heterologous ssDNA (7kb) is tweezed between flow cell bottom and magnetic bead. This requires a different preparation of the magnetic construct.

Magnetic beads are washed additionally (to the standard procedure described in 3.2.3) in detergent containing buffer to increase the binding efficiency of single beads. It is necessary to do so, since the binding efficiency of ssDNA to the flow cell bottom is low and beads which stick to each other reduce the number of usable tethers. After incubation of the magnetic beads with dsDNA (7kb) which have the biotin and DIG label on the same strand, one strand is chemically separated with NaOH. Thereafter, the dissociated strands are washed out repetitively in TE-buffer and the beads are passivated with bio-BSA. Subsequently, the beads are flushed into the designated channel of the flow cell and appropriate tethers (single ssDNA molecules) are found and characterized. Since ssDNA is not coilable, the characterization described in 3.2.4 is not applicable and distinction of single and multiple ssDNA tethers is performed via their force response (fig.14b).

#### 3.2.6. Assay 3 and Assay 5

While the same types of DNA are used, assay 3 ((MT)ssDNA·RecA-heterologous dsDNA(OT)) is the geometrical inversion of assay 2 (3.2.5). Hence, RecA monomers do not assemble on  $\lambda$ -dsDNA tethered between two

Following fishing (fig.11 step 2), the optical construct is moved into the RecA channel where the distinction between single or multiple  $\lambda$ -dsDNA tethered between the optical beads is made by force extension curves (fig.13a). During this procedure the RecA channel is flushed with the same buffer as used for the  $\lambda$ -dsDNA solution. After characterization of a single dsDNA between the two optical beads, RecA containing buffer is flushed into the channel (fig.11 step 3). The rate of RecA filament formation on dsDNA is dependent on the stretching force applied on the DNA molecule (fig.15a). The  $\lambda$ -dsDNA·RecA-

### 3. Material and Methods

optical beads, but on ssDNA (7kb) tweezed between the bottom of the flow cell and a magnetic bead (fig.8). This requires a change of the flow cell configuration (fig.12).

The magnetic beads are prepared and characterized according to the procedure presented for the build up of assay 2. Here, RecA monomer containing buffer is flushed into the same channel as the magnetic beads leading to the formation of RecA-NPF on ssDNA (fig.12 step 2). The mechanics of the assembly of RecA on ssDNA is shown in figure 15b. After full assembly of a ssDNA·RecA-NPF, a low concentration RecA buffer (interaction buffer) is flushed into the channel (fig.12 step 3). This should counteract the disassembly of the RecA from the ssDNA observable in buffers with no RecA. Before fishing for dsDNA

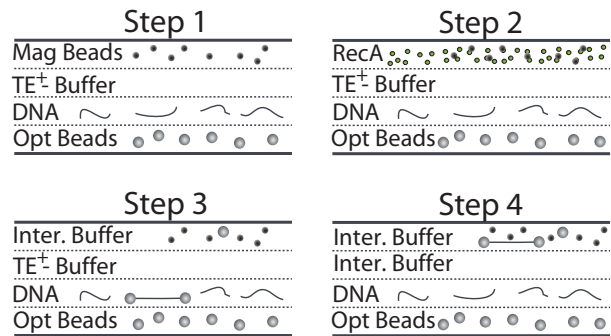


Figure 12: Build up of assays with magnetically tweezed RecA-NPF

an optical reference bead is placed in the vicinity of an appropriate magnetic construct (fig.12 step 3). The optical construct is moved into the magnetic bead channel after fishing (fig.12 step 4). The concentration of RecA monomers in the interaction buffer is so low that no filament assembly takes place on the dsDNA (48kb) construct (fig.24b).

The preparation and characterization of the constructs in assay 5 ((MT)ssDNA·RecA-homologous dsDNA(OT)) follow entirely the one described for assay 3. However, the heterologous ssDNA (7kb) magnetic construct is replaced by 12kb homologous ssDNA to the middle section of the  $\lambda$ -dsDNA.

#### 3.2.7. Assay 4

Assay 4 involves optically tweezed 20kb ssDNA·RecA and a homologous 10kb dsDNA magnetic construct ((OT)ssDNA·RecA-homologous dsDNA(MT)). The flow cell configuration in assay 4 does not differ from the one described for the assay 1 (fig. 11). Here, short homologous dsDNA (20kb) is used to produce ssDNA as substrate for RecA-NPF formation.

After successful fishing for single dsDNA (20kb) force-driven strand separation is achieved by overstretching (fig. 13b). The difference in force response of ds and ssDNA is highlighted in figure 13b. The use of shorter dsDNA is motivated by a higher throughput in ssDNA formation (48kb and 24kb have been tested). Longer dsDNA is more likely to have nicks which lead to breakage of the molecule during force-driven strand separation. The remaining ssDNA after strand separation is the substrate for the subsequent RecA-NPF formation. Like in 3.2.4 this is done by flushing in free RecA monomer containing buffer in the adjacent channel of the magnetic bead channel (fig. 11). After formation, the RecA-NPF on ssDNA (20kb) is brought into the vicinity of the magnetically tweezed heterologous, coilable dsDNA (12kb) (fig.10).

### 3.3. Biophysical Characterization of the Constructs

Next to the accurate three-dimensional manoeuvrability of the different traps and the control of the buffer conditions, the characterization of the constructs prior to the experiments is of utmost importance. To avoid artifacts, one has to make sure that only a single molecule is tethered in the optical and magnetic constructs. In this section we describe how we confirmed RecA filament growth and how we distinguished between multiple and single tethers and between ds- and ssDNA during the formation of the previously described assays.

#### 3.3.1. Characterization of the Optical Constructs

Throughout the experiments, different molecules were manipulated by the optical tweezers. These were bare  $\lambda$ -dsDNA, RecA-NPF formed on  $\lambda$ -dsDNA and RecA-NPF formed on 20kb long ssDNA. Measurements to discern between multiple and single tethered DNA molecules between the optical beads were performed for all of the three constructs. The well known force response of dsDNA upon stretching is a good parameter of determination (fig 13) [28].

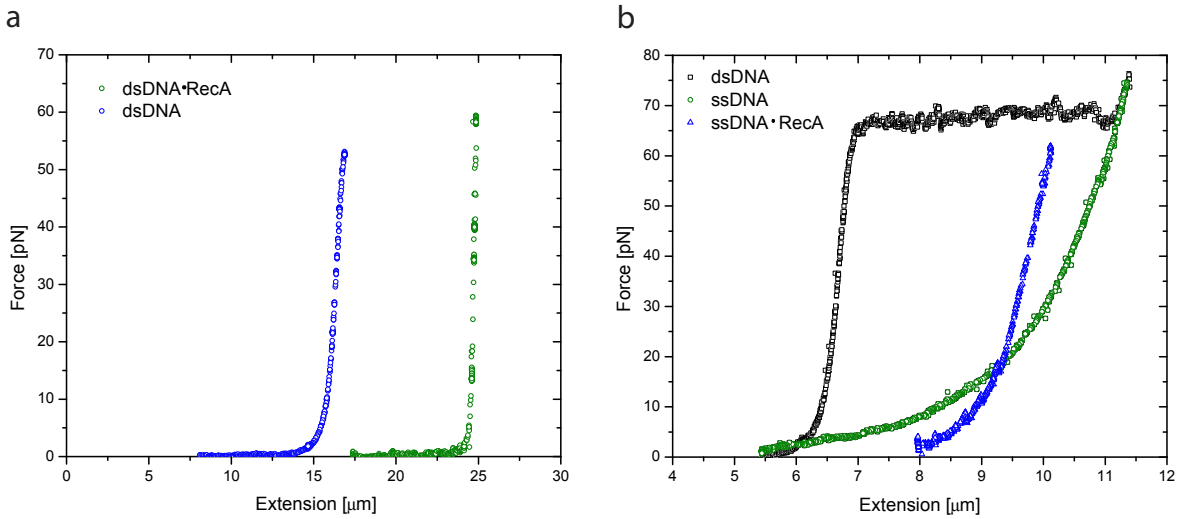


Figure 13: Force versus extension curves. **a**, ( $\lambda$ -DNA) the elastic behaviour of dsDNA below 65pN is described (0.1% accuracy) by a worm-like-chain (WLC) model ( $L_p \sim 50\text{nm}$ ,  $L_0 = 16.49\mu\text{m}$ ). dsDNA·RecA-NPF is  $\sim 12$  times stiffer and  $\sim 1.5$ -fold elongated. **b**, (20kb) at 65pN dsDNA undergoes a conformational transition (overstretching) towards 1.7 times its contour length, within one of the strands eventually peels off (force-induced melting). Above 65pN, ds- and ssDNA have equal extension (ssDNA-regime). At  $\sim 19\text{pN}$  ssDNA·RecA-NPF and ssDNA adapt the same average base length. Because ssDNA·RecA is stiffer than ssDNA the extension of the filament decreases with respect to ssDNA above  $\sim 19\text{pN}$

The elastic behaviour of dsDNA reveals distinct regimes, which are probed by DNA stretching experiments. The force response of dsDNA upon stretching to a overstretching plateau ( $\sim 65\text{pN}$ ) [29],[30] can be described by the worm-like-chain model (WLC) [31], [32].

At very low stretching forces  $F$  ( $F \ll \frac{k_B T}{L_p}$ ) the DNA molecule behaves like a self-avoiding random walk, best described by the model of a freely-joint-chain (FJC) with a contour length ( $L_0$ )

$$F = \frac{3k_B T}{2L_p} \frac{x}{L_0} \quad (5)$$

with  $k_B$  the Boltzmann constant,  $T$  the temperature,  $L_p$  the persistence length and  $x$  the end-to-end distance of the DNA. The random walk behaviour refers to entropical effects. A polymer in aqueous buffer adopts a random coil confirmation that maximizes its entropy [33]. The end-to-end  $x$  distance of the molecule is

### 3. Material and Methods

therefore shorter than its contour length  $L_0$ . Due to this conformational entropy the DNA molecule acts like a hookean spring (entropic spring) at low pulling forces.

The end-to-end distance of the dsDNA approaches its contour length asymptotically at high forces ( $F \gg \frac{k_B T}{L_p}$ ) [34]. Thus, the WLC's relative extension tends towards 1:

$$\frac{x}{L_0} \approx 1 - \frac{1}{\sqrt{F}} \quad (6)$$

In this regime intrinsic effects of the dsDNA molecule govern the elastic response. The phosphate backbone of the dsDNA is stretched into a deformed conformation. Between those two extremes, there is no analytical formula for the force versus extension (FE) behaviour. Instead, an interpolation formula describes the intermediate-force regime with an accuracy better than 0.1%

$$F = \frac{k_B T}{L_p} \left[ \frac{x}{L_0} + \frac{1}{4(1 - \frac{x}{L_0})^2} - \frac{1}{4} + \sum_{i=2}^7 \alpha_i \left( \frac{x}{L_0} \right)^i \right] \quad (7)$$

with  $\alpha_2 = -0.516422$ ,  $\alpha_3 = -2.737418$ ,  $\alpha_4 = 16.07497$ ,  $\alpha_5 = -38.87607$ ,  $\alpha_6 = 39.49944$  and  $\alpha_7 = -14.17718$  [35].

The force versus extension curves are fitted with this numerical solution to extract the contour length  $L_0$  and persistence length  $L_p$ . Assuming an extension of 0.34nm per base pair, the calculated contour length of  $\lambda$ -dsDNA (48502bp) and 20kb dsDNA are 16.49 $\mu$ m and 6.8 $\mu$ m respectively (fig.13a). The persistence length of B-DNA at physiological conditions is found to be  $\sim$ 50nm in previous studies [36]. The number of molecules stretched between the optical traps can therefore be determined by fitting the force response to the numerical WLC solution. For example, two molecules tethered between the optical beads are twice as stiff as a single molecule and as a consequence the persistence length is halved [34].

Under physiological conditions dsDNA undergoes a conformational transition at  $\sim$ 65pN (fig.13b) and the elastic response differs dramatically from the previously described asymptotical approach to the contour length. The DNA elongates  $\sim$ 1.7 times the contour length. The force required to reach the overstretching transition depends on the stability of the DNA double helix and is thus sequence, salt, pH and temperature dependent. The structure of the DNA during this overstretching transition (OT) remains a matter of debate. In one model, the dsDNA cooperatively unwinds and loses the stability provided by base-pair stacking [37]. The bases of the two strands are thought to remain paired in a different conformation than Watson-Crick, viz. forming a ladder rather than a double helix (S-DNA). In a competing model, the hydrogen bonds of the base pairs break and single DNA strands are formed [38], [39]. The base pairs break spontaneously due to the force-induced destabilization of the base stacking. Because base pair breakage is a cooperative effect one of the strands is progressively unpeeled. It has been shown that the unpeeling of one strand from the other favorably initiates from nicks or free DNA ends [39].

However, recent studies revealed that unpeeling (strand separation) or overextension (S-DNA formation) can be selected by changes in molecule environment [40]. Reaching the end of the OT (at  $\sim$ 1.7 times the contour length), the force response of the overstretched dsDNA converges to the one of ssDNA (ssDNA-regime, fig.13b). By releasing the stretching force (from the end of the OT back to the  $<$ 65pN regime) the DNA undergoes the reverse transition. Three different responses can be observed depending on buffer conditions and ramp speed: A slow hysteretic transition (one strand was partially unpeeled during OT and reanneals), a fast non-hysteretic transition (either the DNA obtained S-conformation during the OT, the bases restack and the B-DNA double helix is recovered faster than the time resolution or the reannealing of a partially unpeeled strand is faster than the time resolution) and typical ssDNA force response (one strand was completely

### 3. Material and Methods

unpeeled during OT). The responses on reverse transition can be selected by tuning the buffer conditions (pH, ionicity, temperature) and the stretching parameters (ramp speed and waiting time in the ssDNA-regime). The probability of unpeeling is increased at conditions which are known to destabilize dsDNA (low pH and salt concentration, high temperature). We used a low salt, low pH buffer (see app. B) and a waiting time,  $w_t$ , in the ssDNA-regime of  $1s < w_t < 3s$  to form 20kb ssDNA by force-induced melting (fig.13b).

#### 3.3.2. Characterization of the Magnetic Constructs

Six different molecules were manipulated by the magnetic tweezers. These were bare 7kb ssDNA heterologous and 12kb ssDNA homologous to  $\lambda$ -dsDNA, RecA-NPF formed on 7kb and 12kb ssDNA, 10kb dsDNA heterologous to  $\lambda$ -dsDNA and 10kb homologous to the previously described 20kb ssDNA optical construct. As for optically tethered molecules is it crucial for all constructs to involve only one molecule. Determination between magnetic beads tethered via multiple and single dsDNA molecules was performed by the response of the magnetic construct on torsional stress (fig.14a). dsDNA and ssDNA were distinguished by their different elastic response upon stretching (fig.14b).

The topology of dsDNA can be described by two quantities called twist and writhe. For torsionally constrained (prevented from rotate freely) DNA the sum of twist  $T_w$  and writhe  $W_r$  becomes a topological invariant which is called linking number  $L_k$  [41]

$$L_k = T_w + W_r \quad (8)$$

The twist  $T_w$  of the molecule is the number of times the two strands of the DNA wrap around each other. For relaxed B-DNA, the distance from crossing point to crossing point (pitch) of the double helix is known to be 10.5bp ( $\sim 3.4$ nm). In other words, the twist of a relaxed B-DNA molecule  $T_{w0}$  is the number of helical steps ( $T_{w0} = L_0 / 3.4\text{nm} = \text{bp} / 10.4$ ). The writhe  $W_r$  counts the number of times the helix axis wraps around itself. The canonical example of  $W_r \neq 0$  are the interwound structures of twisted phone cords. We are assuming that torsionally relaxed DNA forms no coils or loops ( $W_{r0} = 0$ ). Hence, for relaxed DNA the linking number  $L_{k0}$  is equal to the number of twists  $T_{w0}$ ,  $L_{k0} = T_{w0}$ .

The behaviour of dsDNA under torsional stress can be described numerically by changes in the linking number of relaxed DNA,  $L_{k0}$ . A DNA molecule is called supercoiled when  $L_k \neq L_{k0}$ . According to equation (8), only changes in twist  $T_w$  or writhe  $W_r$  can account for an excess or deficit in linking number  $\Delta L_k = L_k - L_{k0}$ . Thus, the difference in linking number can be stored by modifying the helical pitch ( $\Delta T_w = T_w - T_{w0}$ ) and by forming interwound structures called *plectonemes* ( $W_r \neq W_{r0} \neq 0$ , fig.14). At a certain torsional stress (buckling transition), the formation of plectonemes is energetically favoured over inducing or removing twist and  $W_r \neq 0$  (fig.14). The density of supercoils  $\sigma$  is defined as the normalized measure of the number of links added to or removed from the molecule [36]

$$\sigma = \frac{\Delta L_k}{L_{k0}} = \frac{\Delta T_w + W_r}{L_{k0}} \quad (9)$$

The molecule is underwound when  $\sigma < 0$  (negatively supercoiled) and overwound when  $\sigma > 0$  (positively supercoiled). Stretching of negatively supercoiled DNA prevents it from relaxing its torsional stress by writhing. The only remaining alternative is to locally denature and thereby relaxing its twist partially (fig.14a) [32], [42]. Local denaturation corresponds to the formation of a bubble along which the two strands are separated and no longer wrap around each other. The linking number of a bubble is zero ( $\sigma_{\text{bubble}} = -1$ ). This enables a small denaturated region of the DNA molecule to absorb a large part of the linking number deficit  $\Delta L_k < 0$  [43]. The remaining non-denaturated parts of the DNA are nearly torsionally relaxed and thus behave globally like torsionally relaxed molecules (fig.14a) [43].

### 3. Material and Methods

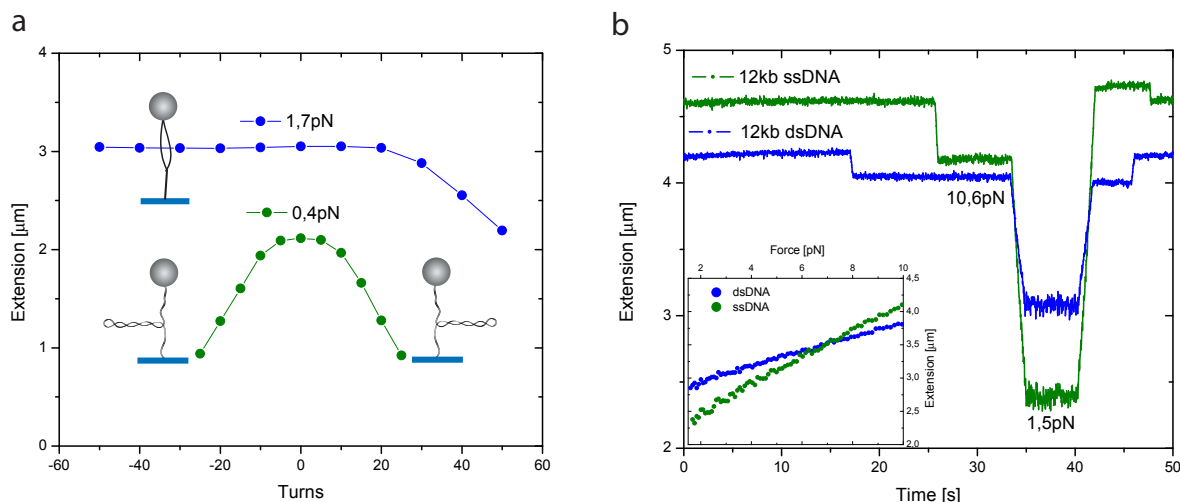


Figure 14: Rotation curves and force response comparison. **a**, rotation curves of 10kb dsDNA at 1.7pN and 0.4pN respectively (20mM Tris 6.85pH,5mM EDTA). At 0.4pN the DNA buckles at  $|\sigma| \sim 0.005$  respectively, and plectonemes are induced. At 1.7pN bubbles are induced for  $\sigma < 0$ , while the buckling transition for positive supercoiling shifts to higher  $\sigma$  values ( $\sigma \sim 0.02$ ). **b**, different force response of ds- and ssDNA in magnetic tweezer constructs. The difference in extension and decay time to the equilibrium position (e.g. from 10.6pN to 1.5pN) are used to distinguish between ds- and ssDNA. Magnetic tweezer calibration (fig.5) and ramp velocity (1mm/s) allow to extract force versus extension curves (Inset). The ds- and ssDNA have equal extension at  $\sim 7$ pN.

This behaviour of underwound DNA allows to distinguish between single and multiple tethered magnetic beads (fig.14a). The extension of single, negatively supercoiled DNA at high enough forces (depending on ionicity, pH and temperature) is insensitive to changes in the molecules linking number. On the other hand, multiple DNA molecules tethered to magnetic beads will braid around each other. Therefore the extension (the height of the magnetic bead) will decrease by inducing negative turns even at high forces.

By anchoring both ends, linear B-DNA is prevented from rotating freely and equation (8) is valid. We realise this in our assay by rotationally clamping the end of one strand to the bottom of the flowcell and the other end of the other strand to the magnetic bead. Therefore we can modify the linking number  $Lk$  and have access to *plectonemes* formation by rotating the magnetic beads (by rotating the external magnets) at low force (here, 0.4pN) and are able to induce bubbles by applying torsional stress at high enough force (here, 1.7pN)(fig.14a). Discrimination of ds- and ssDNA was carried out by their different force response upon stretching (fig.14b). In force versus extension (FE) measurements the noise in x-direction is averaged over a certain time (usually ranging from 1s-30s) and used to calculate (eq.(3)) the force acting on the magnetic bead in z-direction ( $F_{mag}$ ) at a certain height (extension). FE measurements can take up to 30min, depending on the accuracy of the force determination and the number of recorded data points. Given the short lifetime of ssDNA magnetic constructs, characterization by force versus extension curves limits the experimental throughput. Therefore, the difference in contour length at a certain force and the difference in time reaching the equilibrium position (decay time) from one force to another were used to distinguish between ss- and dsDNA (fig.14b). FE curves can be extracted by use of the magnet position-force curve (fig.5) and the ramp speed of the magnetic tweezer (1mm/s)(fig.14b).

#### 3.3.3. RecA Nucleoprotein Filament Formation

RecA assembly on optically trapped  $\lambda$ -DNA was performed at constant forces. As mentioned before, dsDNA in the PBS of a RecA-NPF elongates  $\sim 1.5$  times (fig.13, sec.2.3). A force feedback loop was implemented to

### 3. Material and Methods

compensate the decrease in stretching force upon elongation of the dsDNA during RecA assembly. Figure 15a shows the non-linear rate dependence of filament formation on applied tension. The relative rate of extension ( $\Delta\text{Extension}/\text{Contour Length}\cdot\text{Time}$ ) is accelerated near the overstretching plateau ( $> 50\text{pN}$ ), indicating the higher affinity of RecA monomers to pre-deformed dsDNA (fig.15a). The inset in figure 15a shows the comparison of example traces of the RecA-NPF formation on  $\lambda$ -dsDNA at 55pN and 13.5pN.

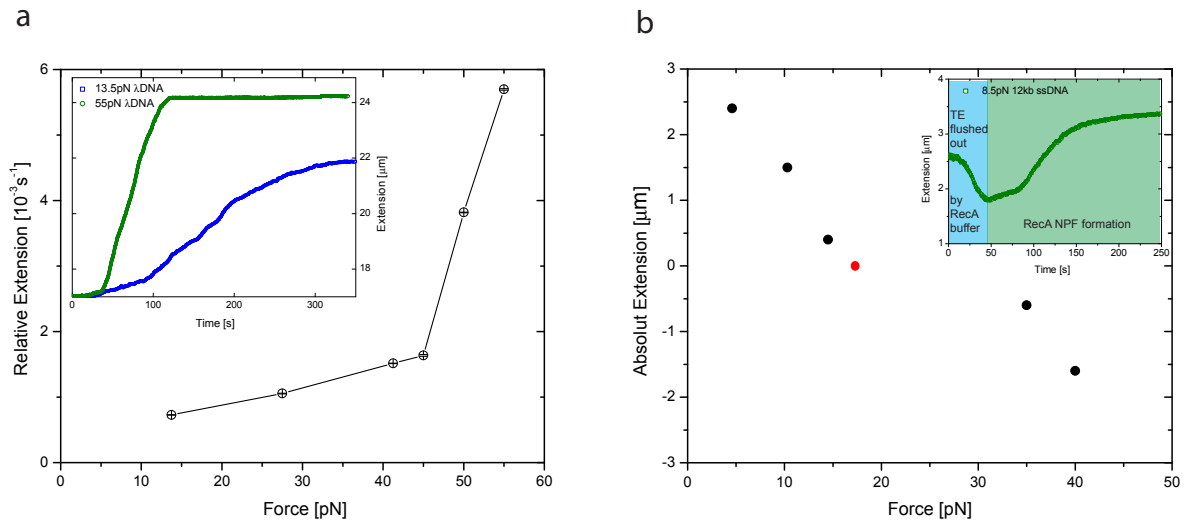


Figure 15: Force dependence of RecA-NPF formation. **a**, The relative rate of extension ( $\Delta\text{Extension}/\text{Contour Length}\cdot\text{Time}$ ) depends non-linearly on the applied tension during the filament formation. The inset shows an example trace of fast RecA assembly on  $\lambda$ -DNA at 55pN. **b**, depending on the applied tension, a (optically trapped 20kb) ssDNA·RecA-NPF is elongated or shortened with respect to bare ssDNA. The data reflects the length difference at certain forces before and after filament assembly. The red data point is the crossing of the ssDNA and ssDNA·RecA FE curves in fig.13b. The inset shows the effect of TE and RecA containing buffer exchange prior to the filament formation on magnetically tweezed 12kb ssDNA

Formation of ssDNA·RecA-NPF's was performed on optically and magnetically tweezed ssDNA. Depending on the applied tension during RecA assembly the NPF is elongated or shortened (fig.15b) with respect to the bare ssDNA. ssDNA·RecA have the same extension when the average base extension in ssDNA reaches  $5.1\text{\AA}$  (depending on buffer and tension) (fig.13b and fig.15b). Therefore, RecA assembly at  $\sim 20\text{pN}$  shows no effect on the contour-length, but only on the stiffness. However, the stiffness of ssDNA·RecA formed under ATP- $\gamma$ -s condition, can be lower than expected (fig.13b). It is possible that the filament is not formed uniformly and that parts of the ssDNA remain RecA free. To avoid this effect *in vivo*, active disassembly of the RecA is driven by ATP hydrolysis after which continuous filament formation can initiate again. In our experiments, hydrolysis driven disassembly does not take place since we use non-hydrolysable ATP- $\gamma$ -s as a cofactor for filament assembly. The average base length of ssDNA depends strongly on the buffer conditions. For example, switching from a low to a high salt buffer leads to a decrease in end-to-end distance due to the formation of secondary structures. Therefore, the extension decreases upon flushing out TE-buffer (no salt) with RecA containing buffer (50mM NaCl, 1mM MgCl<sub>2</sub>) (inset of fig.15b). After the initial decrease, RecA assembly (in case of the shown assembly trace at 8.5pN) start to extend the ssDNA.

### 3.4. Dual Molecule Experiments

Dual-molecule experiments were carried out on the assays described in the sections above (3.2.4-3.2.7). The individual manipulation of two single molecules provides the possibility to perform different types of experiments. In this work we performed

- push-probe experiments to investigate binding energies between RecA-NPFs and DNA molecules by force spectroscopy
- sliding experiments to quantify the friction between different constructs

#### 3.4.1. Push-Probe Type of Experiments for Force Spectroscopy

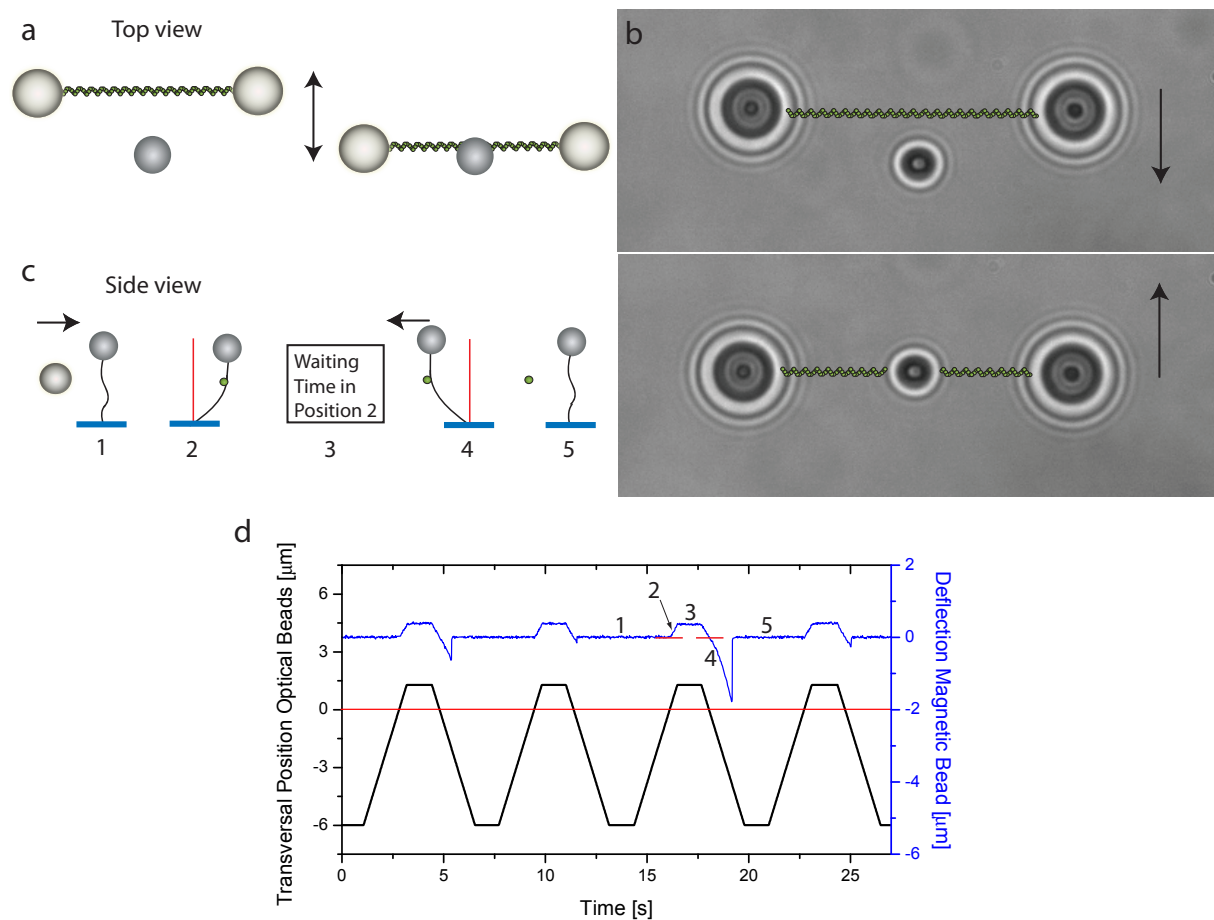


Figure 16: Push-probe type of experiments. The optical construct is repetitively brought into contact with the magnetic construct. Here an example assay with the RecA-NPF formed between the optical beads is shown. **a**, schematic top-view drawing with the movements indicated by arrows. **b**, top-view pictures of constructs out-of-contact (top) and in-contact (bottom). **c**, schematic side view drawing with the movements indicated by arrows. The optical construct is brought into contact with the magnetic construct (1 and 2). The optical construct is pulled back (4) after a certain waiting time wt (3). Eventually binding between the molecules occurred and the magnetic bead is displaced from its equilibrium position (indicated with a red bar in 2 and 4). The bond ruptures at a certain deflection and the magnetic bead snaps back to the equilibrium position (5). **d**, data of a push-probe experiment involving the traces of the transversal movement of the optical beads (black trace, crossing of the equilibrium position of the magnetic bead is indicated with a red line) and of the deflection of the magnetic bead out of its equilibrium position upon pushing and probing (blue trace, the different stages of the push-probe movement according to **c** are indicated)

### 3. Material and Methods

The optical construct is brought into contact with the magnetically tweezed molecule by a transversal movement (fig.16). Eventually contact leads to the formation of a stable joint between the two molecules. If no bond is created, the magnetic bead remains at its equilibrium position upon retraction of the optical construct. If a bond is established, the magnetic bead will follow the movement of the optical construct and will be deflected from the equilibrium position. The displacement of the magnetic bead out of its equilibrium position can be measured and converted into the force which is acting on the bond at the rupture point. This enables the possibility to perform dynamic force spectroscopy by repetitively probing the binding force at different pulling speeds (ramp speed). The height of the beads in respect to their references on the flow cell bottom and thus the height between optical and magnetic beads is kept constant.

#### 3.4.2. Sliding Experiments for Friction Tribology

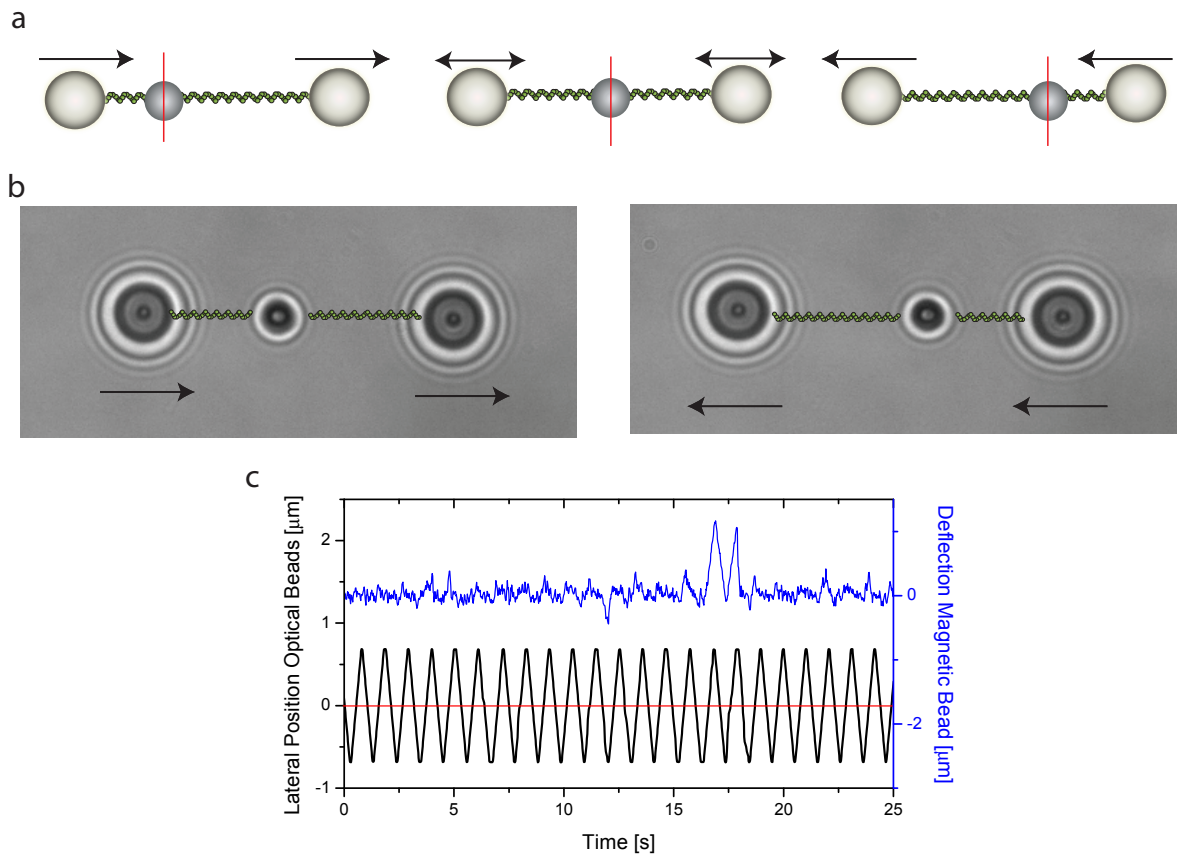


Figure 17: Sliding type of experiments. The optical construct slides repetitively back and forth while being in contact with the magnetic construct. Here an example assay with the RecA-NPF formed between the optical beads is shown. **a**, schematic top view drawing with the movement indicated by arrows. The molecules are arranged such that the magnetic bead in equilibrium position (indicated by a red bar) is located in the middle of the sliding range (cartoon in the middle). The RecA-NPF is then slid back and forth in lateral direction. **b**, top view pictures of constructs at left most (left) and right most (right) positions during a sliding experiment. **c**, data of a sliding experiment involving the traces of the lateral movement of the optical beads (black trace, crossing of the equilibrium position of the magnetic bead is indicated with a red line) and of the deflection of the magnetic bead out of its equilibrium position during sliding (blue trace)

The optical construct is slid back and forth while remaining in contact with the magnetic construct (fig.17). The movements in sliding experiments are performed in lateral direction, perpendicular to the movement in push-probe type of experiments (compare fig.17 with fig.16). This enables possible interactions at every

### 3. Material and Methods

contact position along the optical construct addressed by the sliding movement. The lateral displacement of the magnetic bead from the equilibrium position during sliding is a measure for the strength of the interactions between the two molecules. Eventually stick-slip behaviour as in tribology experiments is observed, indicating binding and unbinding between the two molecules during the sliding movement. The displacement of the magnetic bead due to stick-slipping can be converted into the corresponding force which is acting in lateral direction on the magnetic bead. Thus, the standard deviation of the force acting on the magnetic bead is a measure for the binding probability and strength between two molecules sliding across each other. The height of the beads in respect to their references on the flow cell bottom and thus the height between optical and magnetic beads is kept constant. Sliding experiments were performed on all assays.

## 4. Results

Experimental control (ramp speed, bead heights, scan range etc.) and data acquisition was performed with a custom made LabView program. The three-dimensional control of the optical traps was used to establish contact between two molecules (sec. 3.2). In all measurements, forces acting on the magnetic and the optical constructs were determined by the deflection of the magnetic bead out of its equilibrium position. Although we use soft molecule linkers (ss- and dsDNA), the description of the magnetic construct as an inverted pendulum [25] is valid in the here performed dual-molecule experiments (see below). Therefore, we can directly extract the lateral (x- and y-direction) trap stiffness  $k_x$  (note  $k_x=k_y$ ) from the applied force  $F_{\text{mag}}$  (known from the magnet height, fig.5) and the height of the magnetic bead with respect to the flow cell bottom  $l$  (equal to the end-to-end distance of the linking molecule  $l$ , known from videomicroscopy),  $k_x=F_{\text{mag}}/l$ . Data processing during experiments was done in Matlab, postprocessing in OriginPro.

We first examined the interactions of heterologous dsDNA and ssDNA magnetic constructs with the SBS of a RecA-NPF formed on dsDNA tweezed between optical beads (assay 1 and assay 2). We compared those to interactions between a RecA-NPF with a ssDNA core tethered in the magnetic tweezer and a heterologous dsDNA optical construct (assay 3). In the end we studied the interplay between homologous constructs. For this purpose, the RecA-NPF was formed on a ssDNA magnetic construct and brought into contact with a homologous dsDNA optical construct and vice versa (assay 4 and assay 5, tab.2, fig.8). In the subsequent sections results from dual-molecule experiments on the previously introduced assays are presented one by one.

Table 2: The previously introduced assays which were realised in this work. In the subsequent sections results from sliding and push-probe type of experiments on those assays are presented one by one

Assay Number	Magnetic Construct	Optical Construct
1	heterologous dsDNA	dsDNA · RecA
2	heterologous ssDNA	dsDNA · RecA
3	ssDNA · RecA	heterologous dsDNA
4	homologous dsDNA	ssDNA · RecA
5	ssDNA · RecA	homologous dsDNA

### 4.1. Results: Assay 1

A model has been proposed where the RecA-NPF is thought to actively deform (underwind) an incoming, undamaged dsDNA such that its conformation enables base pairing with the highly deformed ssDNA in the primary binding site (PBS) of the RecA-NPF [48]. However, we could not detect any interaction between  $\lambda$ -dsDNA·RecA-NPF and torsionally relaxed, 10kb heterologous dsDNA during push-probing and sliding experiments (fig.18 and fig.19). The lack of detectable joint formation between the two molecules at low torsional stress, provides first evidence that the RecA-NPF has no active role in binding dsDNA in a deformed conformation. Since the PBS is occupied with a  $\lambda$ -dsDNA, there are no bases in the PBS accessible and interactions with the incoming dsDNA are limited to the secondary binding site SBS of the  $\lambda$ -dsDNA·RecA-NPF. Therefore, a more specific statement can be made: There is no active destabilizing role of the SBS observable if the PBS is occupied with a dsDNA molecule.

The traces of push-probe experiments do not reveal any detectable interactions for torsionally relaxed 10kb DNA ( $\sigma=0$ ) (fig.18a). However, for increasing negative supercoil density ( $\sigma < 0$ ) the probability of binding between the  $\lambda$ -dsDNA·RecA SBS and 10kb dsDNA increases (fig.18b).

#### 4. Results

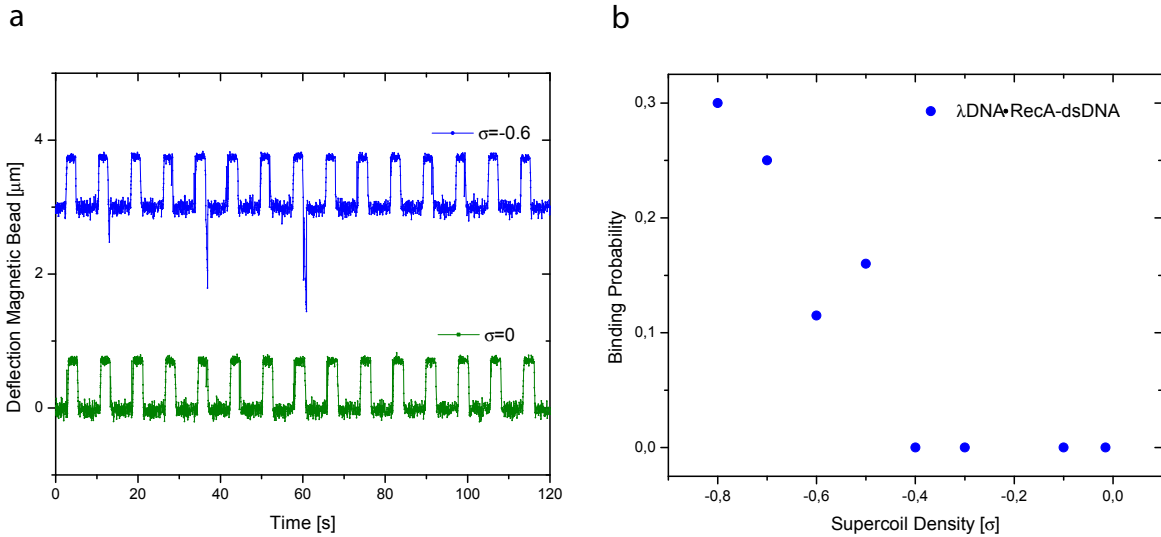


Figure 18: No interactions at low torsional stress detectable. **a**, sample traces of push-probe type of experiments reveal that the probability (number of snapping events/number of approaches) of binding between the SBS of a  $\lambda$ -dsDNA·RecA-NPF and dsDNA (10kb) depends on the applied torsional stress. Here,  $\sigma=0$  and  $\sigma=-0.6$  are shown ( $N=15$ ). **b**, combined data of push-probe experiments at different negative supercoil densities shows that the probability of intermolecular interactions between dsDNA·RecA and dsDNA depends on the applied torsional stress. (each data point  $N=10$ , force loading rate= $1\text{pN}/\mu\text{m}$ ,  $F_{\text{mag}}=2.5\text{pN}$ )

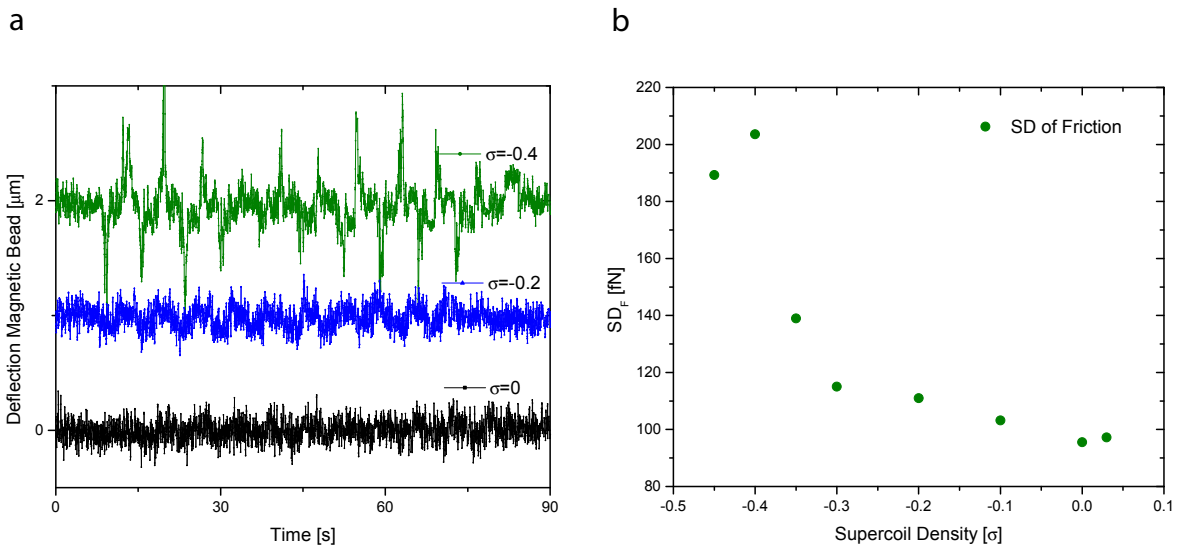


Figure 19: The secondary binding site has no destabilizing role. **a**, sample traces of sliding type of experiments show the same trend like the data from push-probe experiments. Above  $\sigma=-0.2$  thermal fluctuations dominate the bead motion. The intermolecular friction increases for  $\sigma < -0.2$ , indicating binding and unbinding between  $\lambda$ -dsDNA·RecA-NPF and dsDNA. **b**, the standard deviation of the measured forces,  $SD_F$ , increases as a function of negative torsional stress. The deviation in force approaches the thermal noise force ( $\sim 80\text{fN}$ ) at low negative supercoil density (each data point  $N=10$  sliding movements, scan range= $4.965\mu\text{m}$ ,  $F_{\text{mag}}=2.5\text{pN}$ , bandwidth= $50\text{Hz}$ )

Data of sliding experiments show the same trend: the increase in friction (stick-slipping) at negative supercoil densities higher than  $|\sigma| \approx 0.2$ , indicates intermolecular binding and unbinding. At negative torsional stress lower than  $|\sigma| \approx 0.2$  and  $F_{\text{mag}}=2.5\text{pN}$ , frictionless sliding is observed and the force that acts on the magnetic

#### 4. Results

bead is set by thermal fluctuations (fig.19). The standard deviation of the measured force  $SD_F$  ( $\propto$  deflection of the magnetic bead out of the equilibrium position as a function of the supercoil density  $\sigma$ ) becomes larger than the thermal noise for  $\sigma < -0.2$  (fig.19b). At high magnetic forces ( $F_{\text{mag}}=2.5\text{pN}$ ) denaturation compensates the applied negative torsional stress on the 10kbp dsDNA. From the strong dependence of intermolecular interactions on the negative supercoil density of the dsDNA at high force ( $F_{\text{mag}}=2.5\text{pN}$ ), we conclude that the SBS of the  $\lambda$ -dsDNA·RecA-NPF has a preference for ssDNA over dsDNA.

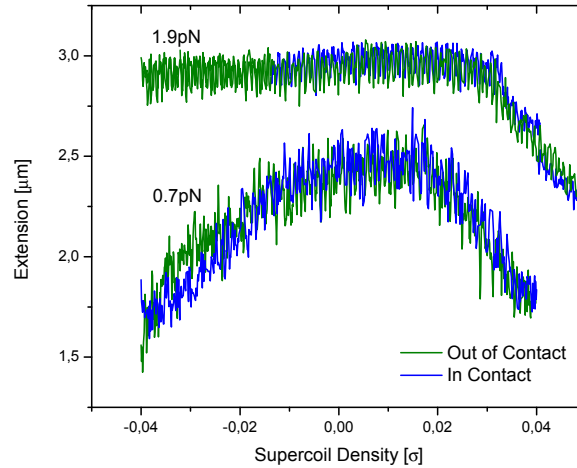


Figure 20: End-to-end distance versus supercoil density. Rotation curves of 10kb dsDNA measured in and out of contact with a dsDNA·RecA-NPF reveal no evidence for active local unwinding of heterologous dsDNA (10kb) (We repeated this experiment four times). The rotations curves overlap over the entire range at high ( $F_{\text{mag}}=1.9\text{pN}$ ) and low force ( $F_{\text{mag}}=0.7\text{pN}$ )

At low force ( $F_{\text{mag}}=0.7\text{pN}$ ) and negative torsional stress the 10kb DNA buckles and forms plectonemes (fig.20). Local unwinding of the 10kb construct by interaction with the SBS would have an effect on the total number of links of the DNA molecule. For example, unwinding of one helical turn corresponds to a reduction in the twisting number of one ( $\Delta Tw=-1$ ). However, the linking number of the construct is invariant, since the 10kb dsDNA is torsionally constrained (clamped between the bottom of the flow cell and the magnetic bead) (sec. 3.3.2). As consequence, a positive change in writhe has to compensate the reduction in twist ( $\Delta Wr=+1$  for  $\Delta Tw=-1$ ). In other words, local unwinding of negatively supercoiled DNA at low stretching force ( $F_{\text{mag}}=0.7\text{pN}$ ) by interactions with the SBS of the RecA-NPF would lead to the release of loops in *plectonemes* in other parts of the molecule. Therefore the end-to-end distance of the dsDNA would change depending on the size and the number of released loops ( $\Delta l_{\text{loop}} \approx 50\text{nm}$ ). We did not find any difference in the length versus coiling behaviour of heterologous 10kb dsDNA in and out of contact with a dsDNA·RecA nucleoprotein filament. In other words, contact between the two constructs did not lead to a change in the end-to-end distance of a negatively supercoiled dsDNA ( $\sigma < 0$ ,  $F_{\text{mag}}=0.7\text{pN}$ ). We therefore conclude, that the interactions between the SBS of a  $\lambda$ -dsDNA·RecA-NPF and a heterologous dsDNA do not lead to local unwinding of the incoming dsDNA as suggested by data from bulk assays [48].

## 4.2. Results: Assay 2

We confirmed the preference of the SBS for ssDNA over dsDNA between optically clamped dsDNA·RecA and magnetically tweezed 7kb heterologous ssDNA. Push-probe experiments showed consistent binding between the secondary binding site (SBS) of the  $\lambda$ -dsDNA·RecA-NPF and incoming ssDNA (fig.21a). This allows dynamic force-spectroscopy (DFS) measurements by iteratively establishing and rupturing the intermolecular bonds at different ramp speeds. Again, the measured signal is the deflection of the magnetic bead out of the equilibrium position. Since the NPF is formed on heterologous dsDNA ( $\lambda$ -dsDNA·RecA), only interactions between the SBS and ssDNA are probed.

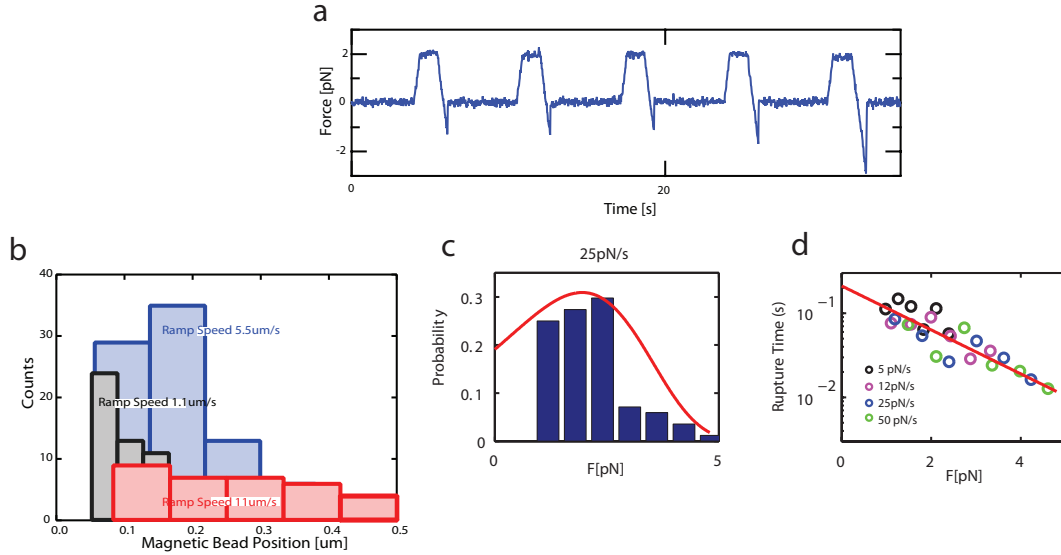


Figure 21: Force-spectroscopy on SBS-ssDNA bonds. **a**, a trace acquired from push-probe experiments between dsDNA·RecA and heterologous ssDNA shows consistent binding. **b**, deflections of snapping events for different push-probe speeds (ramp rate) are distributed, since the rupture of bonds is a stochastic process. Slower ramp rates lead to narrower distributions and smaller most probable rupture deflections. **c**, deflection distributions can directly be converted into rupture force distributions, where the most probable rupture force is given by the maximum of the distribution. **d**, the characteristic bond lifetime  $\tau_0=0.2\text{s}$  and minimum-to-barrier distance  $x_b=2.4676\text{nm}$  can be extracted by Dudko's analysis [46]

Non-covalent bonds like SBS-dsDNA have limited, characteristic lifetimes  $\tau_0$  and spontaneously dissociate ( $k_{\text{off}}=1/\tau_0$ ). Spontaneous unbinding on the time scale of our push-probe measurements (50-100Hz), is thermally activated. Therefore, a Boltzmann ansatz can be used to describe the lifetime by the natural oscillation frequency  $\tau_{\text{osc}}$  (frequency of attempts, set by the thermal energy  $k_B T$ , to overcome the energy barrier, set by the binding energy  $E_b$ ),  $\tau_0 = \tau_{\text{osc}} \exp\left[\frac{E_b}{k_B T}\right]$ . If, upon contact, a bond between  $\lambda$ -dsDNA·RecA-NPF and the ssDNA is established, than retraction of the optically tweezed filament will exert a force on the SBS-ssDNA bond and as a result the lifetime of the bond will be shortened. In the framework of an energy landscape, a bond can be pictured as a local, three-dimensional potential well. Hence, there are many paths out of this energy minimum, which can differ in barrier height and distance of the bottom of the well to the top of the barrier (along a certain path). We are choosing the path of escape and thus the reaction coordinate by applying a force in a certain direction, effectively reducing the three-dimensional potential well to a single energy barrier. The lifetime of a bond loaded with a force depends on the characteristic lifetime  $\tau_0$ , the applied force  $f$  and the minimum-to-barrier distance  $x^\ddagger$  [44]

$$\tau(f) = \tau_0 \exp\left[\frac{-x^\ddagger f}{k_B T}\right] \quad (10)$$

#### 4. Results

We are applying a constant ramp rate (the optical traps move with constant velocity 600nm/s-11 $\mu$ m/s). Furthermore, we make use of a constant force loading rate,  $dF/dt=\dot{F}$ , although we are using molecular linkers with a non-linear elastic response. Two effects allow us to approximate the force loading rate as constant. First, thermally activated contributions affect mostly the region near the dissociation point. Second, in the regime of the applied magnetic force ( $F_{\text{mag}}=13.2\text{pN}$ ), the elastic response of the ssDNA over the range of measured magnetic bead deflections (max. 3 $\mu$ m) is small. We are therefore able to directly convert the measured deflection  $\Delta x$  of the rupture events (fig.21a) into the corresponding rupture force,  $F_{x,\text{rupture}} \approx k_x \Delta x = \frac{F_{\text{mag}}}{l} \Delta x$ .

The rupture of the bond itself is a stochastic process and the rupture deflection  $p(x)$  (fig.21b) and force  $p(F)$  (fig.21c) are therefore distributed. The probability of bond survival  $N(t)$  is expressed in a first-order rate equation,  $\dot{N}=-k_{off}(F(t))N(t)$  [44]. The most probable rupture force is then given by the maximum of the distribution  $p(F)$ . The distribution of the rupture forces is related to the distribution of lifetimes by  $-\dot{N}dt=p(F)dF$  [45] and for a constant loading rate  $\dot{F} \neq \dot{F}(F)$  given by

$$p(F) = \frac{\exp\left[\int_0^F (\dot{F}\tau(f))^{-1} df\right]}{\dot{F}\tau(F)} \quad (11)$$

The width of the distribution increases with the loading rate  $\dot{F}$  and becomes narrower at lower loading rates closer to the equilibrium ( $F=0$ ) (fig.21b shows  $p(t)$  for 1.1 $\mu$ m, 5.5 $\mu$ m and 11 $\mu$ m,  $p(t) \propto p(F)$ ). The rupture force histogram for a constant force loading rate of 25pN/s is shown in figure 21c ( $N=84$ ). From the relation of  $p(F)$  with the loading rate  $\dot{F}$  and lifetime at a constant force  $\tau(F)$  (eq.11), one can extract the bond lifetime at a constant force  $\tau(F)$  in terms of  $p(F)$  and  $\dot{F}$  [46]

$$\tau(F) = \int_F^\infty \frac{p(f)df}{[\dot{F}p(F)]} \quad (12)$$

This equation shows how rupture-force histograms  $p(F)$  measured at different loading rates (here,  $\dot{F}=5\text{pN/s}$ , 12pN/s, 25pN/s and 50pN/s) can be directly transformed into the force dependence of the lifetime  $\tau(F)$ , as it would be measured in a constant-force experiments [46]. According to equation (12), data obtained at different constant loading rates  $\dot{F}$  must collapse onto a single master, curve in case the kinetics at a constant force behave like a single-exponential (eq.10). The slope of the single-exponential in a semi-log plot is then equal to the  $x_b$  and by extrapolating the single-exponential towards  $F=0$ , one can obtain the natural lifetime at zero force  $\tau_0$  (fig.21d). We extract a minimum-to-barrier distance of 2.5nm and a natural lifetime of 200ms from our DFS measurements on bonds between the SBS of a  $\lambda$ -dsDNA·RecA NPF and a ssDNA molecule ( $F_{\text{mag}}=13.2\text{pN}$ , buffer conditions [20mM] Tris-HCl buffer (pH 6.85), [10mM] NaCl, [13mM] MgCl at 21°C).

## 4.3. Results: Assay 3

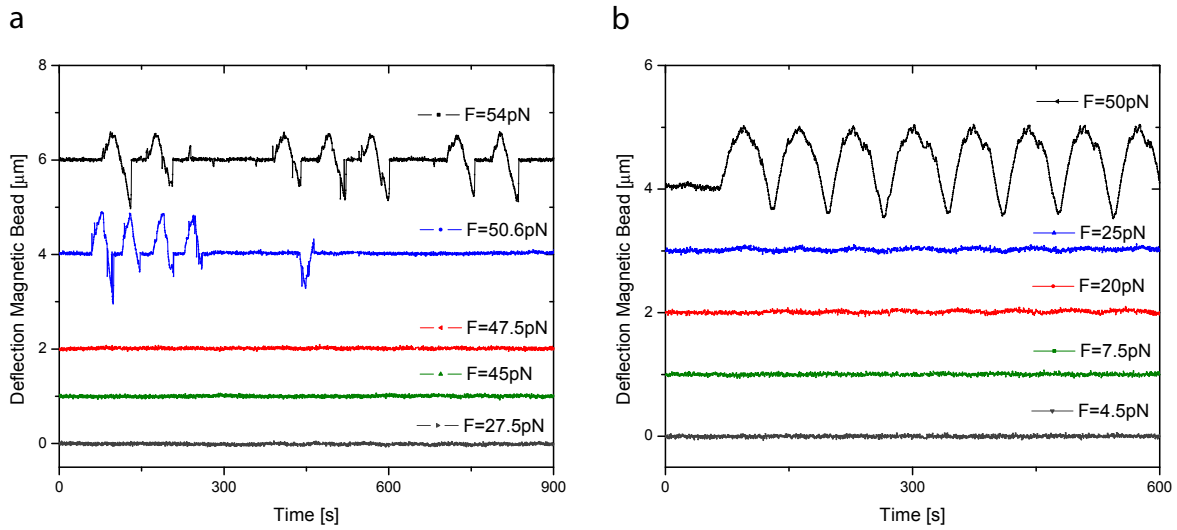


Figure 22: Comparison of interactions between heterologous dsDNA and heterologous dsDNA and ssDNA. **a**, sliding of dsDNA across ssDNA. Binding requires stretching forces close to the overstretching plateau. **b**, sliding of  $\lambda$ -dsDNA across a ssDNA·RecA-NPF. Stable joint formation requires comparable tension on the dsDNA as binding between bare ssDNA and dsDNA

In assay 3, an optically clamped is brought into contact with a RecA-NPF formed on a magnetically tweezed, heterologous ssDNA (7kb). Therefore, we could not induce supercoils in the dsDNA and hence lacked the capability to destabilize dsDNA using torsional stress. Instead, the  $\lambda$ -DNA molecule was gradually destabilized by increasing the stretching force. We performed push-pull and sliding experiments at different stretching forces to investigate the effect of destabilization of the incoming  $\lambda$ -dsDNA on the interactions with the ssDNA·RecA-NPF. However, the RecA-NPF is formed on a ssDNA molecule heterologous to  $\lambda$ -dsDNA. Hence, base pairing between destabilized  $\lambda$ -dsDNA and ssDNA in the PBS can be excluded. In other words, the intermolecular interactions are governed by the SBS of the ssDNA·RecA-NPF. Assay 3 can therefore be compared with assay 1, which allows direct investigation of the effect of the presence of ssDNA in the PBS (assay 3) instead of dsDNA (assay 1).

Figure 22 compares the stretching-force dependence of the friction measured in sliding experiments between 7kb ssDNA·RecA and  $\lambda$ -dsDNA and between bare 7kb ssDNA and  $\lambda$ -DNA respectively. We could not detect any evidence of intermolecular interactions between 7kb ssDNA·RecA and  $\lambda$ -dsDNA below tensions of 40pN (fig.22). We find no evidence that interactions with SBS of a RecA-NPF formed on ssDNA actively destabilize incoming heterologous dsDNA, whether the Rec-NPF is formed on ss- or dsDNA. Therefore, we exclude an allosterical effect of the type of heterologous DNA (ss or ds) in the PBS on the binding properties of the SBS. Active unwinding of the incoming dsDNA by interactions with the SBS, such that its conformation enables base pairing with the highly deformed ssDNA in the primary binding site (PBS), would require several  $k_B T$  of deformation energy (to overcome base pair stacking and locally stretching to match the conformation of the ssDNA in the PBS). If this is the case, than the energy gain upon binding to the SBS must overcome the deformation energy and we could measure stable bonds between relaxed dsDNA and heterologous ssDNA·RecA-NPF's. We find the requirement of destabilization for stable joint formation between RecA-NPF's (ssDNA·RecA in assay 3 and dsDNA·RecA in assay 1) and heterologous dsDNA. Therefore, we conclude that the RecA-NPF has no active role in binding dsDNA in a deformed conformation in the early events leading to recognition.

#### 4.4. Results: Assay 4

The measurements on assay 4 involve a 10kb dsDNA, tweezed in the magnetic trap and a homologous 20kb ssDNA·RecA-NPF, tethered between the optical beads. The single-stranded optical construct was formed by force induced melting as previously described (sec. 3.3.1). We investigated the dependence of the binding probability on torsional stress by push-probe type of experiments. Two major observation can be made. First,

we find that negative supercoiling ( $F_{\text{mag}}=0.68\text{pN}$ ) strongly enhances the binding probability. We observed binding events for torsionally relaxed dsDNA ( $p=0.2$ ,  $N=20$ ,  $\sigma=0$ ) and a rapid increase of the binding probability with minor changes of the supercoil density ( $p=0.75$ ,  $N=20$ ,  $\sigma=-0.005$ ) (fig.23a). Consistent binding was detected at low negative torsional stress ( $p=1$ ,  $N=16$ ,  $\sigma=-0.015$ ). We can compare the here acquired data with the data obtained on assay 1 ((OT)dsDNA·RecA-heterologous dsDNA(MT)), since in assay 1, only interaction with the SBS are involved and thus it has no influence whether the constructs are complementary or not. In contrast to assay 1, here we formed the RecA filament on homologous ssDNA, allowing complementary base pairing between the triplet units of the ssDNA in the PBS and incoming dsDNA. We conclude that the large difference in the negative supercoil dependence originates from the availability of complementary base pairing.

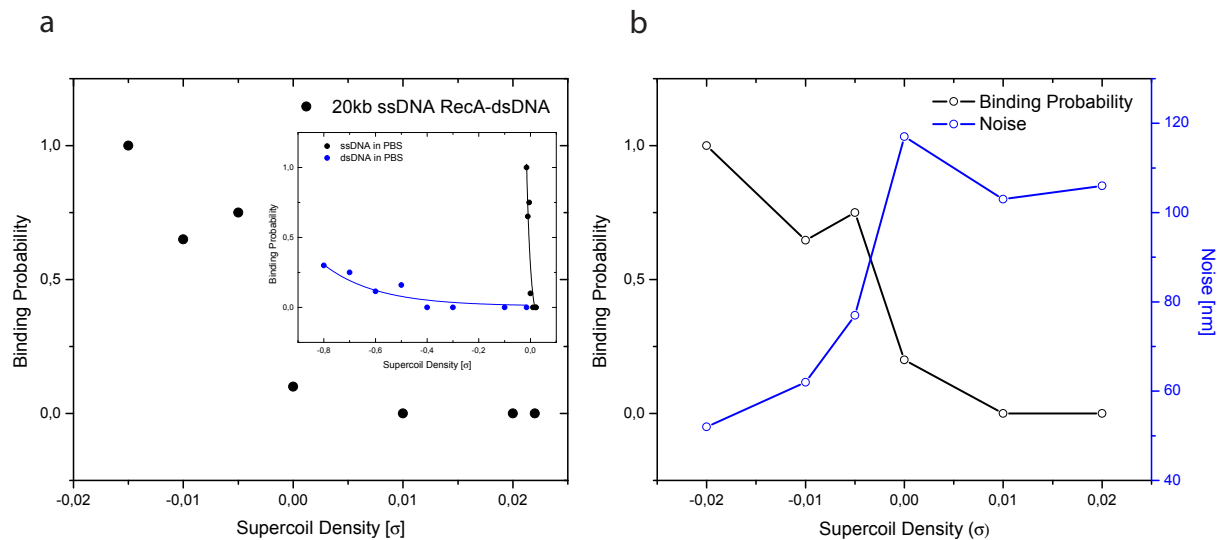


Figure 23: No interactions at low torsional stress detectable. **a**, the probability of binding between ssDNA·RecA-NPF and homologous dsDNA strongly depends on the applied torsional stress on the dsDNA. The inset is a comparison with fig.18b. The large difference in the negative supercoil dependence between heterologous (assay 1, blue data points) and homologous (assay 4, black data points) constructs originates from the availability of complementary base pairing. **b**, the lateral noise on the magnetic bead (averaged over 4s) during the waiting time before retraction in push-probe experiments (fig.16, while the ssDNA·RecA filament is in contact with the magnetically tweezed dsDNA), decreases with increasing negative torsional stress (blue curve). The binding probability upon retraction (black curve, data from **a**) is negatively correlated with the noise level before retraction

We further compared the noise levels during the waiting time (4s) before retracting the ssDNA·RecA-NPF from the dsDNA magnetic construct (fig.23b). We know from the force spectroscopy measurements on assay 2, that the characteristic lifetime of SBS-ssDNA bonds is  $\tau_0 \sim 200\text{ms}$ . Hence, the lifetime of the interactions measured must be larger, because we assume that complementary base pairing contributes an additional binding energy (measurements were performed in the same buffer conditions [20mM] Tris-HCl buffer (pH 6.85), [10mM] NaCl,

#### 4. Results

[13mM] MgCl and at the same temperature, 21°C). However, averaging the noise level while being in contact gives a measure for the binding probability, assuming that the natural off-rate  $k_0$  is lower than the sampling frequency of the camera (50Hz). Indeed, the averaged noise level (4s) before pulling the RecA filament out of contact decreases with increasing negative torsional stress on the dsDNA ( $F_{\text{mag}}=0.68\text{pN}$ ). This indicates more bonds are established during the 4s waiting time for negatively supercoiled DNA.

Second, the most probable rupture forces at aligned (homologous sequences of the 20kb long ssDNA·RecA-NPF and of the incoming 10kb dsDNA encounter each other at the point of contact) and misaligned (homologous sequences are on one strand are not in close vicinity to each other) positions differ. The data set of snapping events which we obtained is too small to allow further analysis (N=14 for aligned and N=27 for misaligned positions). Nevertheless, preliminary data shows the expected trend: Higher rupture forces (longer loading times) for aligned homologous counterparts.

### 4.5. Results: Assay 5

Structural destabilization of dsDNA interacting with the secondary binding site of a RecA-NPF might also be driven by ATP hydrolysis. We are able to exclude this possibility by direct comparison of interactions between magnetically tweezed (12kb) ssDNA·RecA and  $\lambda$ -DNA under ATP- $\gamma$ -s [0.3mM] and ATP [0.3mM] conditions. Sliding type of experiments were first performed in ATP containing buffer, since non-hydrolysable ATP analogs (like ATP- $\gamma$ -s) stick to the binding pocket and do not allow binding of subsequently flushed in, hydrolysable cofactors (like ATP).

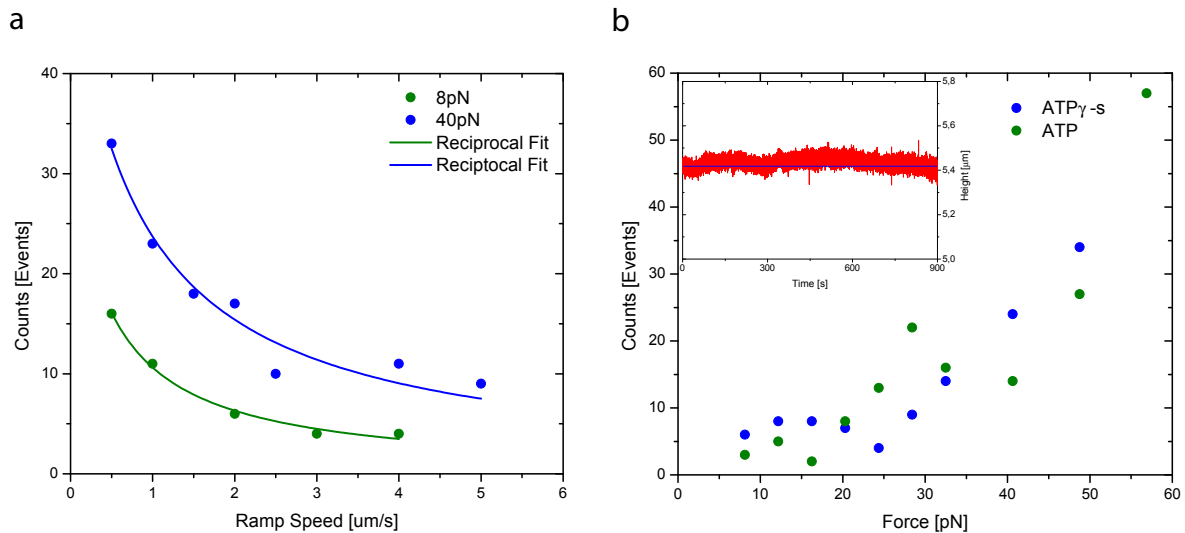


Figure 24: Comparison of sliding experiments of  $\lambda$ -dsDNA across a homologous ssDNA·RecA-NPF under ATP and ATP- $\gamma$ -s conditions. **a**, the number of events per sliding movement shows a reciprocal dependence on the ramp rate. The binding probability (number of events) shifts towards higher values for higher tension on the dsDNA. **b**, the binding probabilities remain under both conditions (ATP versus ATP- $\gamma$ -s) the same. A influence of ATP hydrolysis on the joint formation can therefore be excluded. The binding probability per sliding movement increases under both conditions with increasing stretching force on the  $\lambda$ -dsDNA molecule. The inset shows that the ssDNA·RecA NPF remains stable in a 17nM RecA background (blue line is a guide for the eye)

Sliding experiments show the same trends between experiments on different pairs of molecules. However, a quantitative comparison between measurements on different pairs of molecules requires extensive statistics. On the other hand, experiments under different conditions (ATP versus ATP- $\gamma$ -s) on the very same molecules assure comparability but pose several experimental challenges. The limited lifetime of the ssDNA·RecA magnetic constructs makes it difficult to acquire full data sets in both environments. Under both conditions, a low concentration RecA background is needed to counteract the disassembly of RecA from the ssDNA. RecA assembly on the double stranded  $\lambda$ DNA is known to be enhanced under ATP conditions [13]. We found that a RecA background of [17nM] meets both requirements: No RecA assembly on dsDNA while the ssDNA·RecA-NPF remains stable (fig.24b).

No intermolecular interactions between ssDNA·RecA and relaxed, homologous  $\lambda$ -DNA were observed. As for sliding experiments on assay 3 ((MT)ssDNA·RecA-heterologous dsDNA(OT)),  $\lambda$ -DNA was gradually destabilized by increasing the stretching force. No difference in force dependence between ATP and ATP- $\gamma$ -s conditions has been found (fig.24a, each data point N=20 sliding movements, scan range=3.2 $\mu$ m $\pm$ 0.1 $\mu$ m). Hence, we conclude that ATP hydrolysis plays no role in SBS interactions with incoming dsDNA. The absence of interactions of RecA-NPF formed on both, ss- and dsDNA, with relaxed heterologous or homologous dsDNA

#### 4. Results

under ATP and ATP- $\gamma$ -s conditions, leads to the conclusion, that dsDNA is not actively destabilized, but that spontaneous denaturation in the incoming dsDNA govern SBS-dsDNA interactions.

Figure 24a (each data point  $N=20$  sliding movements, scan range= $3.2\mu\text{m}\pm 0.1\mu\text{m}$ ) shows the dependence of detectable binding events on ramp speed under ATP conditions. The scan range was kept constant, while the ramp rate ( $v_{\text{ramp}}$ ) was varied. Hence, the contact time at a certain point along the  $\lambda$ -dsDNA decreases with increasing  $v_{\text{ramp}}$ , contact time  $\propto 1/v_{\text{ramp}}$ . The probability of binding between the homologous ssDNA·RecA-NPF and a certain point along the  $\lambda$ -dsDNA depends on the time that point is in contact with the RecA-NPF, binding probability  $\propto$  contact time. Hence, the number of events per sliding movement show a reciprocal dependence on the ramp rate (fig.24b, fit for 8pN:  $N(\text{events})=1/((0.0299\pm 0.00363)+(0.0642\pm 5.08686\text{E-}4)*v_{\text{ramp}}$ , fit for 40pN:  $N(\text{events})=1/((0.01941\pm 0.00273)+(0.0228\pm 2,89814\text{E-}4)*v_{\text{ramp}}$ ).

## 5. Discussion

### 5.1. Interpretation of the results

RecA-NPFs are the mediators of the strand exchange in homologous recombination (sec. 2.2). To replace the resected strand of the damaged DNA, one of the strands of an incoming DNA duplex must have access to the bases of the ssDNA overhang in the PBS of a RecA-NPF (fig.1). Hence, experiments performed on RecA-NPF's formed on dsDNA do not allow for investigation of interactions between DNA in the primary binding site (PBS) and the secondary binding site (SBS). The bases of the dsDNA in the RecA-NPF are paired and thus inaccessible. Therefore interactions between the constructs in assay 1 ((OT)dsDNA·RecA-heterologous dsDNA(MT), sec. 4.1) and assay 2 ((OT)dsDNA·RecA-heterologous ssDNA(MT), sec. 4.2) are restricted to the SBS. In other words, the results of push-probe and sliding experiments on these assays give a direct measure of the interaction between the SBS of a RecA-NPF and dsDNA and ssDNA respectively (hereafter, SBS-dsDNA and SBS-ssDNA).

Within the resolution of our experiments, we could not detect any formation of SBS-dsDNA bonds during push-probe experiments. However, consistent binding of ssDNA to the SBS of the dsDNA·RecA was observed. We therefore concluded in line with previous studies, that the SBS has a strong preference for ssDNA over dsDNA [47]. In fact, from the inability to resolve dsDNA-SBS bonds, we conclude that these interactions are at least two orders of magnitude weaker than SBS-ssDNA interactions. To provide further evidence, we locally denatured the magnetically tweezed dsDNA in assay 1 by underwinding it (fig.18a). Indeed, the probability of binding events between the underwound dsDNA and the SBS increased with decreasing supercoil-density ( $\sigma < 0$ ), pointing towards a preference for ssDNA. Furthermore, sliding experiments showed the same behaviour: friction between dsDNA·RecA and dsDNA increases with decreasing supercoil-density, (fig.19). These findings are true for heterologous as well as for homologous dsDNA in the PBS, since only bonds with the SBS were probed.

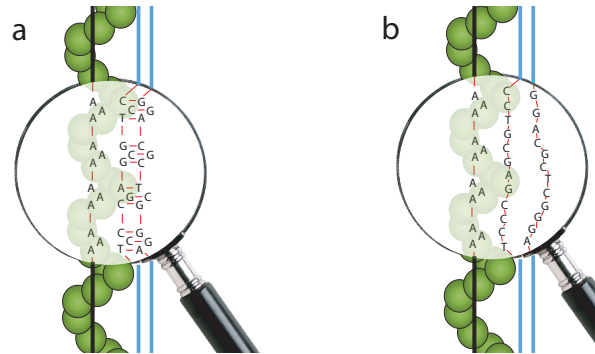


Figure 25: Active destabilization versus spontaneous denaturation. **a**, the common model (of SBS-dsDNA interactions) states that the RecA-NPF actively deforms the incoming dsDNA to allow sampling of the highly deformed ssDNA in the PBS [12], [9], [48]. This is unlikely, since active deformation implies a high binding energy which on the other hand would make a fast search process impossible. **b**, we state that binding of dsDNA to the SBS is governed by spontaneously occurring, denatured regions in the incoming dsDNA (the genome of *E.Coli* is negatively supercoiled  $\sim 0.05\sigma$  [50]). We base this statement on (1) the fact that we could not detect any SBS-dsDNA interactions (2) the strong negative supercoil dependence ( $\sigma < 0$ ) of SBS-dsDNA interaction (indicating that ss-SBS bonds are the first step of the sampling process) and (3) that the search process does not require ATP hydrolysis

Nonetheless, the weak binding affinity of dsDNA to the SBS could also depend on the type of DNA in the PBS, e.g. dsDNA in the PBS might allosterically inhibit binding of dsDNA to SBS. Investigations on assay 3

## 5. Discussion

((MT)ssDNA·RecA-heterologous dsDNA(OT), sec. 4.3) excluded this possibility. We found no differences in the binding probability of dsDNA to the SBS whether there was ss- or dsDNA in the PBS. Unlike for assay 1 and assay 2, the incoming dsDNA was tethered between the optical beads. Therefore, gradual denaturation of the incoming dsDNA was not inducible by underwinding. Instead, force-induced destabilization of basepairing was achieved by increasing the stretching force. At low stretching forces fewer basepairs are disrupted than at high force. Again, we found for the push-probe type of experiments that the probability of SBS-dsDNA bonds increases with increasing stretching force. Additionally, sliding experiments revealed the same trend: friction between ssDNA·RecA and dsDNA was observed to be within the thermal noise level below a certain stretching force on the incoming dsDNA. Summarizing, we find that SBS-dsDNA bonds will not (or very weakly) be established if the dsDNA is not actively destabilized. Thus, the gain of free energy upon binding of dsDNA to the SBS ( $\Delta G_{ds-SBS}$ ) is very small compared to the loss in free energy due to basepair disruption ( $\Delta G_{ds-SBS} \ll \Delta G_{bp}$ ). Nevertheless, binding mediated by the ssDNAs of denaturation bubbles in the dsDNA is only observed at certain level of underwinding and stretching. Before a certain threshold, the binding of ssDNA to the SBS is outcompeted by the nearby complementary ssDNA in the denaturation bubble. We therefore conclude that the gain in free energy upon binding of ssDNA to the SBS is smaller than the basepair energy in a non-distorted B-DNA conformation (fig.26b)

$$\Delta G_{bp} > \Delta G_{ss-SBS} \quad (13)$$

Since the ssDNA in the PBS is in a highly deformed configuration (sec. 2.3), incoming dsDNA has to be underwound and stretched. The common doctrine states that the dsDNA is actively prepared to sample ssDNA in the PBS upon binding to the SBS ([48], [9]). In this model, the gain in free energy by establishing the ds-SBS bond has to account for the energies required for stretching and underwinding the dsDNA. This is unlikely due to the very weak interaction of intact dsDNA and partially denatured dsDNA with the SBS of ssDNA·RecA-NPFs. Furthermore, long-lived, strong ds-SBS bonds would not allow a fast search process.

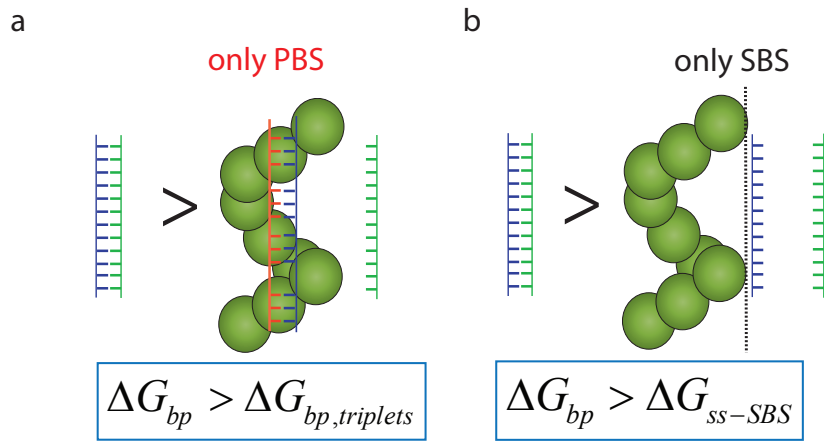


Figure 26: A single bond is not enough. **a**, the heteroduplex in the PBS has to adopt a stretched and underwound conformation [12]. Therefore, complementary base pairing between the ssDNA in the PBS and incoming ssDNA is energetically less favoured than Watson-Crick pairing between the two single strands of a breathing bubble in the incoming dsDNA. We conclude that  $\Delta G_{bp} > \Delta G_{bp, triplet}$ . **b**, prerequisite for establishing SBS-dsDNA interactions are denaturation bubbles, and is therefore rather governed by non-specific binding of ssDNA than of dsDNA. Nevertheless, a high negative torsional stress ( $\sigma=-0.4$ ) is required to observe stable joints. We therefore conclude that the gain in free energy upon binding of ssDNA to the SBS is smaller than the basepair energy in a non-distorted B-DNA conformation,  $\Delta G_{bp} > \Delta G_{ss-SBS}$

Instead, our findings support a model where ss-SBS bonds are the first step of the sampling process. This

## 5. Discussion

requires breathing of the incoming dsDNA, the spontaneous formation of denaturation bubbles, which permits the formation of ss-SBS bonds (fig.25). With DNA breathing as prerequisite, the speed of homology sampling between ssDNA·RecA and dsDNA is set by the breathing dynamics themselves. Therefore the supercoil density of the incoming dsDNA is thought to regulate the speed of homologous pairing, since DNA breathing dynamics are promoted by negative superhelical tension in the DNA [49].

We tested the influence of supercoil density on homologous pairing on assay 4 ((OT)ssDNA·RecA-homologous dsDNA(MT), sec. 4.4) and found, as for assay 1, that dsDNA underwinding strongly stimulates joint molecule formation. We can compare data on supercoil density obtained on interactions in assay 1 and assay 4, since in assay 1 only interactions with the SBS are involved and thus it has no influence whether the constructs are complementary or not. In assay 4 on the other hand, the triplet units of the ssDNA in the PBS (sec. 2.3) are accessible for homologous incoming dsDNA. While in assay binding events are observed at low negative supercoil density ( $\sigma = -0.015$ ) much higher negative superhelical tension is required in assay 1 ( $\sigma = -0.4$ ) (fig.27).

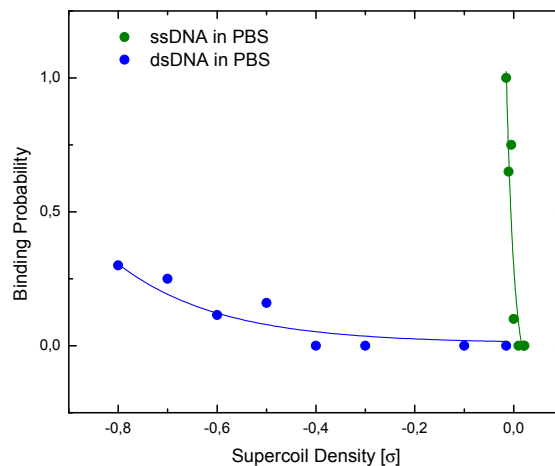


Figure 27: Comparison of the coiling dependence on interactions between ssDNA·RecA-dsDNA and dsDNA·RecA-dsDNA. The probability of binding between ssDNA·RecA-NPF and homologous dsDNA depends stronger on the applied torsional stress on the dsDNA than the probability of binding between dsDNA·RecA-NPF and heterologous dsDNA. The large difference in the negative supercoil dependence between heterologous (assay 1, fig.18b) and homologous (assay 4, fig.23a) constructs originates from the availability of base pairing

The huge discrepancy can be explained by an additional energy contribution from interactions of ssDNA in the PBS with the homologous dsDNA in the SBS. In other words, the ability of Watson-Crick-basepairing between ssDNA in the PBS and dsDNA in the SBS lowers the energy required to form stable joints in comparison to interactions which are restricted to the SBS.

If a homologous dsDNA binds to the SBS via a breathing bubble, one of the strands will bind to the nonspecific (non-sequence dependent) SBS and the other strand will be sampled by the ssDNA in the PBS. Eventually, complementary sequences encounter each other and form a heteroduplex (between the ssDNA in the PBS and the complementary, non-SBS-bound strand of incoming dsDNA) via Watson-Crick-basepairing. The heteroduplex has to adopt a stretched and underwound conformation, since the dsDNA in PBS has a conformation similar to ssDNA [12]. The free energy gain due to formation of a basepair in a triplet unit of the heteroduplex ( $\Delta G_{bp, \text{triplet}}$ ) will therefore be smaller than the energy required to disrupt a basepair in non-distorted B-DNA

## 5. Discussion

$$\Delta G_{bp} > \Delta G_{bp,triplet} \quad (14)$$

This indicates that only by complementary basepairing between the ssDNA in the PBS and one of the strand (hereafter incoming ssDNA) of the incoming dsDNA no stable joint can be formed (fig.26a). Thus, the interaction of the other strand (hereafter outgoing ssDNA) of the incoming dsDNA with the SBS has to compensate the discrepancy between  $\Delta G_{bp, triplet}$  and  $\Delta G_{bp}$ . Hence we can conclude that  $\Delta G_{ss-SBS} > \Delta G_{bp} - \Delta G_{bp,triplet}$  and from the experiments restricted on interaction with the SBS (see above) that

$$\Delta G_{bp} > \Delta G_{ss-SBS} > \Delta G_{bp} - \Delta G_{bp,triplet} \quad (15)$$

This means that stable joints between ssDNA·RecA-NPF and dsDNA are only formed when both binding sites of the RecA-NPF interact with both of the strands of the breathing bubble (fig.28). The incoming ssDNA strand forms a heteroduplex with the ssDNA in the PBS and the outgoing strand binds to the SBS (we refer to this situation as double-grip).

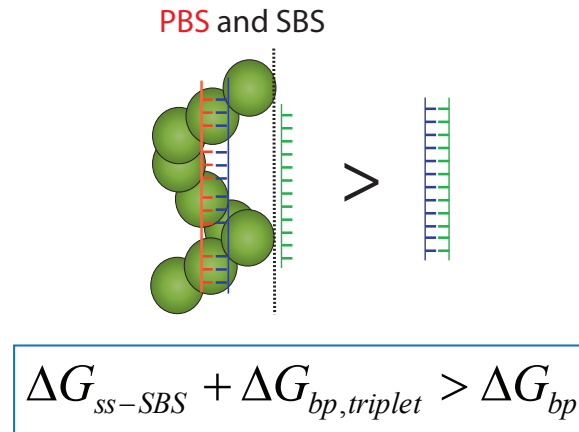


Figure 28: Together we are strong. Stable bonds between a RecA-NPF and incoming dsDNA can only be formed if both strands of a denatured region in incoming dsDNA interacts with the RecA-NPF. In other words, complementary base pairing between incoming ssDNA and ssDNA in the PBS as well as unspecific binding between the outgoing ssDNA and the SBS of the RecA-NPF are necessary to compete with Watson-Crick base pairing of the incoming dsDNA,  $\Delta G_{ss-SBS} + \Delta G_{bp,triplet} > \Delta G_{bp}$

## 5.2. A model for homology recognition

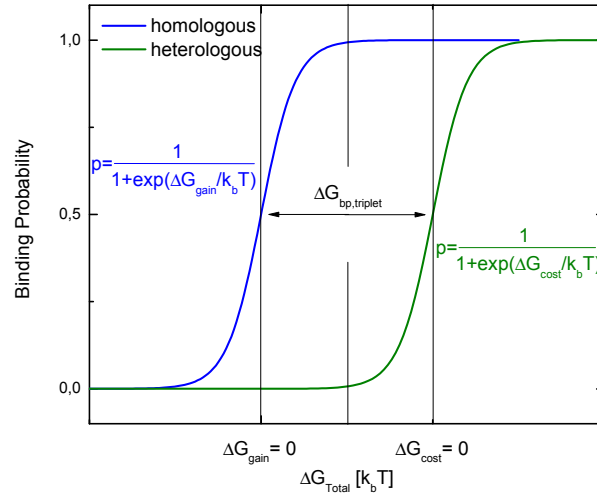


Figure 29: Optimizing the costs. The binding probabilities of homologous and heterologous follow both a Boltzmann distribution of the total energy. The probabilities for  $\Delta G_{\text{gain}}=0$  and  $\Delta G_{\text{cost}}=0$  ( $p=1/2$ ) are setting the range for the optimal total energy. The maximal cost is  $-\Delta G_{\text{bp,triplet}}$ , the maximal gain  $+\Delta G_{\text{bp,triplet}}$ . The optimal balanced cost and gain is  $|\Delta G_{\text{bp,triplet}}|/2$  (high probability for homologous binding, low probability for heterologous binding)

A reasonable assumption is that the energetic features of RecA-NPF ( $\Delta G_{\text{ss-SBS}}$ ,  $\Delta G_{\text{bp,triplet}}$ ) have evolved to efficiently solve the task of homology recognition. Thus, the cost for incorrect detected ( $\Delta G_{\text{cost}}=\Delta G_{\text{ss-SBS}}-\Delta G_{\text{bp}}<0$ ) and the gain for correct detected sequences are optimized ( $\Delta G_{\text{gain}}=\Delta G_{\text{ss-SBS}}-\Delta G_{\text{bp}}+\Delta G_{\text{bp,triplet}}>0$ ). Heterologous as well as homologous binding will be bistable (binding probability=1/2), if binding to homologous sequences (correct detection) is not rewarded ( $\Delta G_{\text{gain}}=0$ , binding to the SBS and PBS exactly accounts for the base pair breakage) and the binding to heterologous sequences is not penalized ( $\Delta G_{\text{cost}}=0$ , SBS accounts alone for the loss in free energy due to base pair breakage). Therefore, the optimal total energy gain must be between 0 and  $\Delta G_{\text{bp,triplet}}$ . Assuming a balanced distribution of cost and gain ( $|\Delta G_{\text{gain}}|=\Delta G_{\text{cost}}$ ), one can see from figure 29 that the optimum is in the middle of the possible range,  $\Delta G_{\text{gain,optimal}}=1/2\Delta G_{\text{bp,triplet}}$ . It follows that the optimal energy gain upon binding to the SBS is  $\Delta G_{\text{optimal,ss-SBS}}=\Delta G_{\text{bp}}-1/2\Delta G_{\text{bp,triplet}}$ . From equation (14) we know that  $\Delta G_{\text{bp,triplet}}<\Delta G_{\text{bp}}$  and from the distorted structure of the hetero duplex we guess the energy gain upon formation of a basepair in a triplet unit ( $\Delta G_{\text{b,triplet}}$ ) to be around  $\sim 0.7\Delta G_{\text{bp}}$

$$\Delta G_{\text{bp,triplet}} \approx 0.7\Delta G_{\text{bp}} \Rightarrow \Delta G_{\text{ss-SBS}} \approx 0.65\Delta G_{\text{bp}} \quad (16)$$

In order to probe for homology, the incoming ssDNA must bridge the gap between the SBS and PBS ( $24\text{\AA}$  -  $27\text{\AA}$ ). This implies that not the entire length of a denaturation bubble (in the incoming dsDNA) interacting with the SBS, searches for homologous sequences in the ssDNA·RecA. Approximately three unpaired bases (referred to as  $x$ , equal to four base-to-base distances) are required to span the distance between PBS and SBS (fig.31), assuming a base-to-base distance of  $6.19\text{\AA}$  (app.D). In total, six base pairs of the incoming dsDNA must be broken to allow sampling of the ssDNA bound to the PBS by the incoming ssDNA (fig.31). While the six bases of the incoming ssDNA span from the SBS to the PBS, the six complementary bases of the outgoing ssDNA bind to the SBS, resulting in a energy deficit of  $6\Delta G_{\text{ss-SBS}}-6\Delta G_{\text{bp}}\approx -2.1\Delta G_{\text{bp}}<0$ . The formation of a stable joint depends therefore exclusively on the interaction of ssDNA·RecA and the incoming strand, and thus on complementary binding. The gain in free energy of Watson-Crick base pairing between the nucleotide

## 5. Discussion

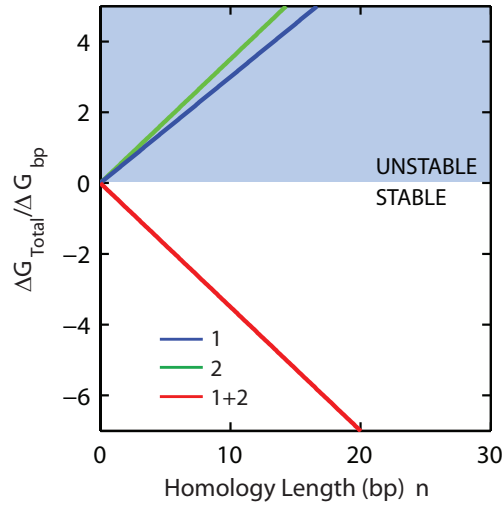


Figure 30: A model for homology recognition. We propose the double-grip model: Interactions with only one binding site of the RecA-NPF are outcompeted by the base pairing of the incoming dsDNA. Stable joints are only formed if both binding sites contribute to the interaction (homologous recognition). This can not be the full mechanism of homologous recognition, since a single complementary base ( $n=1$ ) in the PBS would already be sufficient to form a stable joint and hence, in average, every fourth base would be a match.

triplets in the PBS and incoming complementary together with the interactions between the outgoing ssDNA and the SBS must overcome the lacking  $2\Delta G_{bp}$ . The minimal size of homology required to overcome the energy deficit due to the topological constraint is  $2.1\Delta G_{bp}/(\Delta G_{ss-SBS} + \Delta G_{bp,triplet} - \Delta G_{bp}) \approx 2.1/0.35 = 6 = n$ . The distance between the PBS and SBS, therefore sets a lower limit on the size of homology, necessary to establish a stable bond between a ssDNA·RecA-NPF and incoming dsDNA. In other words, the fidelity of the homology search process is provided by a topological constraint limiting the minimal number of complementary base pairing  $n$  to 6bp. It follows that the minimal size of a denaturation bubble able to probe for homology is  $n+2x=12bp$ .

Denaturation of the incoming dsDNA, induced by tension or torsional stress, affects the fidelity of the recognition by reducing the energy of base pairing  $\Delta G_{bp}$ . The total energy gain upon recognition ( $\Delta G_{gain}$ ) will increase and the number of stable joints will rise with the applied tension (or torsional stress) on the incoming dsDNA. In other words, stretching force and torsional stress have a negative effect on the fidelity of the recognition process and will drive the minimal number of complementary base pairing required for stable joint formation below 6bp. We measured this prediction with sliding experiments on assay 5 ((MT)ssDNA·RecA-homologous dsDNA(OT), sec. 4.5) and concluded that binding becomes less sequence specific, and is taking place at more positions along the ssDNA·RecA-NPF.

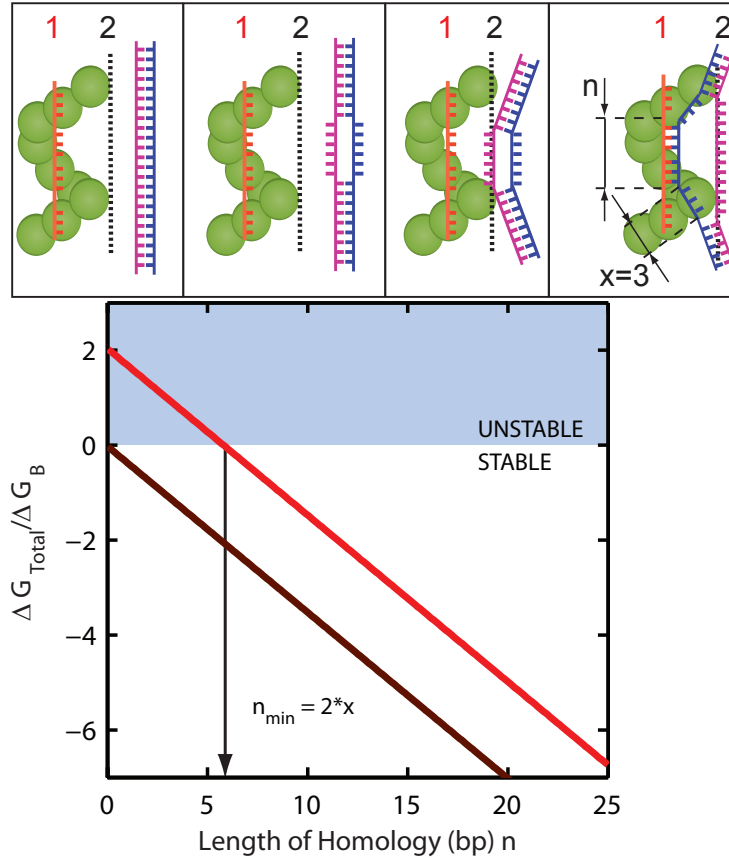


Figure 31: A topological constraint governs the fidelity of the homologous recognition. The incoming ssDNA must overcome the huge gap between the PBS and SBS ( $24\text{\AA} - 27\text{\AA}$ ) [12]. We assume that in the vicinity of the RecA-NPF spontaneous denaturation of a dsDNA occurs (DNA breathing). One of the strands of the bubble undergoes unspecific binding to the SBS the other probes for homology in the PBS (double grip model). Considering the molecular picture, the incoming ssDNA has to bridge the gap between PBS and SBS. Approximately 3 unpaired bases (neither to the SBS nor PBS) are required to span the gap ( $x=3$ ). In total  $2x$  bases must be broken to allow sampling of the PBS-ssDNA. This sets an initial cost  $\sim 2.1\Delta G_{\text{bp}}$  which must be overcome by homologous recognition. Assuming  $\Delta G_{\text{bp,triplet}} \approx 0.7\Delta G_{\text{bp}}$  and  $\Delta G_{\text{ss-SBS}} \approx 0.65\Delta G_{\text{bp}}$  the minimal number of complementary base pairing required to establish a stable joint is  $n=6$

### 5.3. The speed of recognition

Stable joints between a ssDNA·RecA-NPF and incoming dsDNA require the spontaneous formation of denaturation bubbles (fig25). We conclude this from the fact that we could not detect any SBS-dsDNA interactions before a certain level of underwinding ( $\sigma < 0$ ) and stretching. The similar behaviour of force-induced breathing bubbles under ATP and ATP- $\gamma$ -s conditions (assay 5, (MT)ssDNA·RecA-homologous dsDNA(OT)), allows to exclude an active role of hydrolysis upon SBS-dsDNA formation. This gives further, strong evidence that the speed of homologous pairing is set by the breathing dynamics themselves. Therefore the negative supercoil density of the incoming dsDNA (for *E.Coli*  $\approx -0.05\sigma$  *in vivo* [50]) is thought to regulate the speed of homologous pairing. Given the stiffness of the RecA-NPF (fig.13) we assume that not the filament itself, but denaturation bubbles along the dsDNA are the search entity for homology (fig.32).

Taking the possibility of parallel search and the *in vivo* time scale for homology search set by the cell's life cycle ( $\sim 1\text{h}$ , [19]) into account, we can give a rough estimate for the frequency of sampling attempts of single denaturation bubbles.

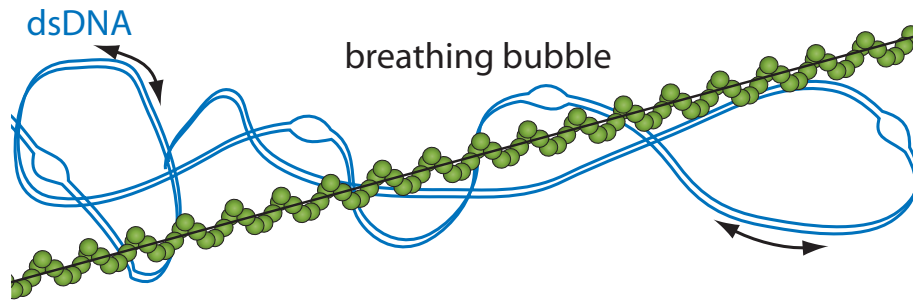


Figure 32: DNA searches for homology. Given the rigidity of the ssDNA·RecA-NPF ( $L_p \approx 600\text{nm}$ ) compared to the stiffness of dsDNA ( $L_p \approx 50\text{nm}$ ) under physiological conditions, it is more likely that the dsDNA and not the NPF is the search entity for homology. In this model, the breathing bubbles diffuse along the dsDNA and are stabilized upon encounter of complementary bases in the PBS of the filament

We assume a RecA-NPF formed on 1kb long ssDNA. Given a minimum search unit of 6bp, the number of sites where stable binding can be established, is  $\sim 167$  ( $1000\text{bp}/6\text{bp}=167$ ). Considering the genome of *E.Coli*,  $\sim 3 \cdot 10^6$  basepairs (G) must be scanned for homology. The numbers of base pairs probed per second is thus given by  $\sim 3 \cdot 10^6 / 3600\text{s}$  which results in a sample frequency of  $\sim 833\text{bp/s}$ . The frequency decreases to  $\sim 5\text{bp/s}$ , assuming simultaneous sampling of all probing sites along the RecA-NPF. We suppose that the minimal probing length of a bubble of arbitrary size is given by the minimal search unit ( $n=6\text{bp}$ ). Thus, the DNA-breathing dependent sampling frequency is

$$f = \frac{G}{N * t * n} \approx 1\text{Hz} \quad (17)$$

## 6. Conclusions

Different types of dual molecule experiments have been performed with different types of constructs. RecA- NPFs have been assembled on ds- and ssDNA tethered between two optical beads (optical construct) or between the bottom of the flow cell and a magnetic bead (magnetic construct). The combination of magnetic tweezers with dual-bead optical traps allowed us to disentangle the mechanisms which allows RecA-NPFs to provide a high-speed and high-fidelity homologous search and recognition process:

- We find no active role for the secondary binding site of RecA-NPFs in destabilizing the helix of the incoming dsDNA. The interactions between dsDNA and RecA-NPFs are very weak. This is true both under ATP (hydrolysable) and ATP- $\gamma$ -s (non-hydrolysable) conditions.
- We find that the probability of homologous pairing can be enhanced by torsional stress. From the strong supercoil density dependence we conclude that breathing bubbles initiate homology sampling.
- The binding of ssDNA to the secondary binding site is orders of magnitudes stronger than the binding of dsDNA. By comparing the interaction dependence on torsional stress and tension between different assay, we were able to conclude that  $\Delta G_{ss-SBS} + \Delta G_{bp,triplet} > \Delta G_{bp} > \Delta G_{ss-SBS}, \Delta G_{bp,triplet}$ .
- We developed a “double-grip” model based on these inequalities. Binding is unstable if not both ssDNA binding sites of the RecA-NPF interact with both strands of a breathing bubble in the incoming dsDNA. The prerequisite of breathing bubbles in the dsDNA to initiate, together with the double-grip requirement to promote homology search allows homologous recognition to take place without energy consumption (ATP hydrolysis).
- The fidelity of the homology recognition process is provided by the topological constraint induced by the gap between the primary and secondary binding site. The fidelity critically depends on the torsional stress and the tension on the incoming dsDNA.
- The speed of the homologous sampling is governed by the breathing dynamics in the incoming dsDNA and the possibility of parallel search. We conclude that the dsDNA and not the RecA-NPF is the search entity during homologous sampling.

## 7. Acknowledgement

First and foremost I would like to thank Iwijn de Vlamincq for his help and support. Your uncomplicated acquaintance made it a pleasure to work in the lab and in the end it was your supervision, which made this work possible. Thanks for giving me such a great time, inside and outside of the lab. Furthermore, I thank Marijn van Loenhout for his advises and motivating ideas along this project. I would like to thank Cees Dekker for giving me the opportunity to work in his group and for all his good advise and Roderick Lim for being my supervisor back in Basel. A special thank to all the other people who helped me out writting this thesis. Jacob Kressemakers for the helpful discussions, Susanne Hage for the help in the biolab, Tom Henighan for the proof reading of the thesis and specially Immanuel Willi for the continuous coffee cap supply for my coffee machine. Thanks everybody for giving me so many great memories.

## References

- [1] Hoeijmakers, J.H., **Genome maintenance mechanisms for preventing cancer**, *Nature*, vol. 411, 366-374, (2001)
- [2] Lindhal, T. and Wood, R.D., **Quality control by DNA repair**, (*Science*), vol. 286, 1897-1905, (1999)
- [3] Friedberg, E.C. *et al.*, **DNA Repair and Mutagenesis**, *Am. Soc. Microbio.*, (1995)
- [4] Rich, T., *et al.*, **Defying death after DNA damage**, *Nature*, vol. 407, 777-783, (2000)
- [5] Schaerer, O.D., **Chemistry and Biology of DNA repair**, *Angew. Chem. Int. Ed.*, vol. 42, 2946-2974, (2003)
- [6] Cromie, G.A. *et al.*, **Recombination at Double-Strand Breaks and DNA Ends: Conserved Mechanism from Phage to Humans**, *Mol. Cell*, vol. 8, 1163-1174, (2001)
- [7] Critchlow, S.E. and Stephen, P.J., **DNA end-joining: from yeast to man**, *Trends Biochem. Sc.*, vol. 23, no. 10, 394-398, (1998)
- [8] Bianco, P.R. *et al.*, **DNA Strand Exchange Proteins: A Biochemical and Physical Comparison**, *Frontiers Biosc.*, vol. 3, 570-603, (1998)
- [9] Savir, Y. and Tlusty, T., **RecA-Mediated Homology Search as a Nearly Optimal Signal Detection System**, *Mol. Cell*, vol. 40, 388-396, (2010)
- [10] Kowalczykowski, S.C. *et al.*, **Biochemistry of Homologous Recombination in *Escherichia coli***, *Microbio. Reviews*, vol. 58, no. 3, 401-465, (1994)
- [11] Stasiak, A. and Di Capua, E., **The helicity of DNA in complexes with RecA protein**, *Nature*, vol. 299, 185-186, (1982)
- [12] Chen, Z. *et al.*, **Mechanism of homologous recombination from the RecA-ssDNA/dsDNA structures**, *Nature*, vol. 453, 389-394, (2010)
- [13] Galletto, R. *et al.*, **Direct observation of individual RecA filaments assembling on single DNA molecules**, *Nature*, vol. 443, 875-878, (2006)
- [14] Kim, J.-I. *et al.*, **On the Role of ATP Hydrolysis in RecA Protein-mediated DNA Strand Exchange**, *J. Bio. Chem.*, vol. 267, no. 23, 16438-16443, (1992)
- [15] Whitby, M.C. and Lloyd, R.G., **Branch migration of three-strand recombination intermediates by RecG, a possible pathway for securing exchange initiated by 3'-tailed duplex DNA**, *EMBO J.*, vol. 14, 3302-3310, (1995)
- [16] Shah, R. *et al.*, **Genetic recombination in *E. coli*: RuvC protein cleaves Holliday junction at resolution hotspots in vitro**, *Cell*, vol. 79, 853-864, (1994)
- [17] Brewer, L.R. and Bianco, P.R., **Laminar flow cells for single-molecule studies of DNA-protein interactions**, *Nat. Methods*, vol. 5, 517-525, (2008)
- [18] Honigberg, S.M. *et al.*, **Ability of RecA protein to promote a search for rare sequences in duplex DNA**, *PNAS*, vol. 83, 9586-9590, (1986)

## References

- [19] Camerini-Otero, R.D. and Hiesh, P., **Parallel DNA triplexes, homologous recombination, and other homology-dependent DNA interactions**, *Cell*, vol. 73, 217-223, (1993)
- [20] den Blanken, J.F., **Development of a hybrid magnetic- and optical tweezers setup**, *Master Thesis*, TU Delft, NL, April 2010
- [21] Ashkin, A. *et al.*, **Observation of a single-beam gradient force optical trap for dielectric particles**, *Opt. Lett.*, vol.11, 288-290, (1986)
- [22] Ashkin, A., **Forces of a single-beam gradient laser trap on a dielectric sphere in the ray optics regime**, *Biophys. J.*, vol.61, 569-582, (1992)
- [23] Neuman, K.C. and Block, S.M., **Optical trapping**, *Rev. Sc. Ins.*, vol. 75, 2787-2807, (2004)
- [24] Tlusty, T. *et al.*, **Optical Gradient Forces of Strongly Localized Fields**, *Phys. Rev. Lett.*, vol.81, 1738-1741, (1998)
- [25] Strick, T.R. *et al.*, **The elasticity of a single supercoiled DNA molecule**, *Science*, vol. 271, 1835-1837, (1996)
- [26] Neuman, K.C. *et al.*, **Single-Molecule Micromanipulation Techniques**, *Annu. Rev. Mater.*, vol. 37, 33-67, (2007)
- [27] te Velthuis, A.J.W. *et al.*, **Quantitative Guidelines for Force Calibration through Spectral Analysis of Magnetic Tweezer Data**, *Biophys. J.*, vol. 99, 1292-1302, (2010)
- [28] Smith, S.B. *et al.*, **Direct mechanical measurements of the elasticity of single DNA molecules by using magnetic beads**, *Science*, vol. 258, 1122-1126, (1992)
- [29] Smith, S.B. *et al.*, **Overstretching B-DNA: The Elastic Response of Individual Double-Stranded and Single-Stranded DNA Molecules**, *Science*, vol. 271, 795-799, (1996)
- [30] Léger, J. *et al.*, **Structural transitions of a twisted and stretched DNA molecule**, *Phys. Rev. Lett.*, vol.83, 1066-1069, (1999)
- [31] Bustamante, C. *et al.*, **Entropic elasticity of lambda-phage DNA**, *Science*, vol.265, 599-600, (1994)
- [32] Marko, J.F. and Siggia, E.D., **Stretching DNA**, *Macromol.*, vol.28, 8759-8770, (1995)
- [33] de Gennes, P.G. **Scaling concepts in polymer physics**, *Cornell University Press*, Ithaca, NY, (1979)
- [34] Strick, T.R. *et al.*, **Homologous pairing in stretched supercoiled DNA**, *PNAS*, vol. 95, 10579-10583, (1998)
- [35] Bouchiat, C. *et al.*, **Estimating the Persistence Length of a Worm-Like Chain Molecule from Force-Extension Measurements**, *Biophys. J.*, vol. 76, 409-413, (1999)
- [36] Strick, T.R. *et al.*, **Stretching of macromolecules and proteins**, *Rep. Prog. Phys.*, vol. 66, 1-45, (2003)
- [37] Cluzel, P., **DNA: An extensible molecule**, *Science*, vol. 271, 792-794, (1996)
- [38] Rouzina, I. and Bloomfield, V., **Force-induced melting of the DNA double helix 1. thermodynamic analysis**, *Biophys. J.*, vol. 80, 882-893, (2001)

## References

- [39] Mameren, J. *et al.*, **Unraveling the structure of DNA during overstretching by using multicolor, single-molecule fluorescence imaging**, *PNAS*, vol. 106, 18231-18236, (2009)
- [40] Fu, H. *et al.*, **Two distinct overstretching DNA states**, *Nuc. A. Res.*, vol. 38, no. 16, 5594-5600, (2010)
- [41] Withe, J., **Self-linking and the Gauss integral in higher dimensions**, *Am. J. Math.*, vol. 91, 693-728, (1969)
- [42] Marko, J.F. and Siggia, E.D., **Fluctuations and supercoiling of DNA**, *Science*, vol. 265, 506-508, (1994)
- [43] Strick, T.R. *et al.*, **Behaviour of Supercoiled DNA**, *Biophys. J.*, vol. 74, 2016-2028, (1998)
- [44] Evans, E., **Probing the relation between force, lifetime and chemistry in single molecular bonds**, *Annu. Rev. Biophys. Biomol. Struct.*, vol. 30, 105-128 (2001)
- [45] Dudko, O.K., *et al.*, **Intrinsic Rates and Activation Free Energies from Single-Molecule Pulling Experiments** *Phy. Rev. Lett.*, vol. 96, 108101/1-4, (2006)
- [46] Dudko, O.K., *et al.*, **Theory, analysis, and interpretation of single-molecule force spectroscopy experiments** *PNAS*, vol. 105, 15755-15760, (2008)
- [47] Mazin, A.V. and Kowalczykowski, S.C., **The function of the secondary DNA-binding site of RecA protein during DNA strand exchange**, *EMBO J.*, vol. 17, 1161-1168, (1998)
- [48] Rould, E. *et al.*, **Unwinding of Heterologous DNA by RecA Protein during the Search for Homologous Sequences**, *J. Mol. Biol.*, vol. 226, 127-139, (1992)
- [49] Frank-Kamenetskii, M., **How the double helix breathes**, *Nature*, vol. 328, 17-18, (1987)
- [50] Sinden, P.R. *et al.*, **Torsional tension in the DNA double helix measured with trimethylpsoralen in living E. coli cells: analogous measurements in insect and human cells**, *Cell*, vol. 21, 773-783, (1980)

## A. Appendix

Outline of the experimental set up described in section 3.1. A detailed description of the build up and the containing elements can be found in J.F. den Blankens master thesis [20].

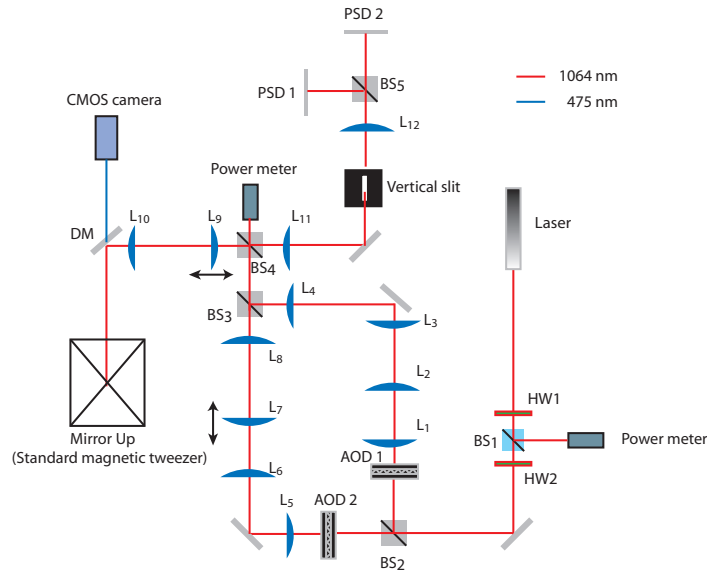


Figure 33: Schematics of the optical pathway

A half-wave plate (HW1) and a polarizing beam splitter (BS<sub>1</sub>) are placed directly after the laser to control the total power of the beam. A second half-wave (HW2) plate is used to tune the ratio of s- and p-polarized light. Two separated beams for individual traps are created by splitting up the different polarizations (BS<sub>2</sub>). Acousto-optical deflectors allow to steer the distinct beams in x- and y-direction. 1:1- telescopes (L<sub>1</sub>-L<sub>2</sub> and L<sub>5</sub>-L<sub>6</sub>) transpose the deflection plane at the AOD's onto two 2:1-expanders (L<sub>3</sub>-L<sub>4</sub> and L<sub>7</sub>-L<sub>8</sub>). The moveable lens L<sub>7</sub> in one of the beam paths allows to change the focus position (z-height) of one of the traps (Trap 1) individually. The beams are combined again at BS<sub>3</sub> and expanded by a factor 1.2 with the lenses L<sub>9</sub> and L<sub>10</sub>. Lens L<sub>9</sub> is used to steer the focus of both beams simultaneously. A power meter behind a beam-splitter (BS<sub>4</sub>) is used as a reference of the trap power. The detection of the position of the optical beads within the optical traps is done by detecting the reflected light from the beads. BS<sub>4</sub> splits the reflected light from the optical tweezers path. The beam diameter is adjusted with L<sub>11</sub> and L<sub>12</sub> to fit the detection area of the position sensitive detectors (PSD's). Simultaneous detection of the bead position in both traps is realized by the separation of the linear polarizations (BS<sub>5</sub>). A vertical slit is placed at the focal distance of L<sub>11</sub> to block reflections from the surface of the flow cell.

## B. Appendix

Procedures and Buffers for the assembly of the assays 3.2 and experiments 4:

### Buffers:

- Optical Bead Wash Buffer  
10mM Tris 6.85pH, 1M KCl, 5mM EDTA 8.0pH
- TE<sup>+</sup>-Buffer  
20mM Tris 6.85pH, 200mM KCl, 5mM EDTA 8.0pH
- TE-Buffer  
20mM Tris 6.85pH, 5mM EDTA 8.0pH
- RecA Binding Buffer  
20mM Tris 6.85pH, 50mM NaCl, 1mM MgCl<sub>2</sub>
- DNA overstretching Buffer  
20mM MES 6.25pH, 100mM KCl
- Interaction Buffer  
20mM Tris 6.85pH, 10mM NaCl, 13mM MgCl<sub>2</sub>
- Flow Cell Storage Buffer  
5 ml PBS buffer, 0.5 ml of Na<sub>2</sub>N<sub>3</sub> (1M), 0.5 ml Tween, 300 ul of BSA (10mg/ml)

Buffers were filtered (0.22  $\mu$ m Millipore<sup>TM</sup> Millex<sup>®</sup> GV filter, PVDF membrane) and prior to experiments degassed at 10<sup>-3</sup>bar for 40min. All syringes of the pressure box have a volume of 3ml. To avoid oxygen radicals, 30 $\mu$ l of DTT (100mM) are added to all buffer solution except for the RecA containing buffer.

### Flow cell preparation (3.2.1):

- Cut out pattern of the flow cell from Parafilm "M"<sup>TM</sup>
- Drill holes (sandblaster) for inlets and outlet in first glass slide (24mmx60mm)
- Sonicate for 10min in EtOH
- Cover second glass slide with 0.1%nitro cellulose in amyl acetate
- Place patterned between the two glass slides and anneal on heating plate (90°)
- Incubate the flow cell with 100mM anti-DIG over night
- Passivate before use with bio-BSA (10mg/ml) for 30min

### Optical beads wash (3.2.1):

Optical Beads are provided by Spherotech Inc., Sphero<sup>TM</sup>Streptavidin Polystyrene (Cat. No. SVP-20-5, 0.5% w/v, 2.16 $\mu$ m, 5ml).

- Filter a 2:1 Bead wash buffer:Bead stock solution through a 50K filter (Millipore<sup>TM</sup> Amicor<sup>®</sup> 0.5ml, regenerated cellulose)by centrifugation (6000rpm, 2min)

## B. Appendix

- Recover the washed beads: put the micro pore tube up-side-down in an Eppendorf tube and centrifuge (6000rpm, 1min)
- Add 900ul bead wash buffer to the eppendorf tube
- Stir it

Stir the beads again, prior to the use of experiment. Mix 200 $\mu$ l with 2.8ml degased TE<sup>+</sup> directly in the syringe.

**Magnetic beads preparation (3.2.3):** Magnetic Beads are provided by InvitrogenDynal AS, Dynabeads<sup>®</sup> MyOne<sup>™</sup>Streptavidin C1 (Cat. No.650.01, 1 $\mu$ m, 10mg/ml, 2ml).

for dsDNA

- Wash 10 $\mu$ l bead stock solution in TE-buffer (Dilute in 50 $\mu$ l TE and extract beads from the solution by holding a permanent magnet in proximity of Eppendorf tube, repeat 2-3x)
- Incubate with 1 $\mu$ l dsDNA for 5-10min (dsDNA stock solution (see app.C) diluted 1:12000 - 1:18000 in TE)
- Incubate with 10 $\mu$ l bio-BSA (10mg/ml) for 15min
- Add 1.5ml TE<sup>+</sup>

The washed magnetic beads (in TE<sup>+</sup>) are transferred to one of the syringes. For DNA incubation the valve of the corresponding syringe is opened for  $\sim$ 10min (dismount magnet head!) and afterwards the channel is flushed with TE-buffer for  $\sim$ 10min. Magnets are installed after no more beads can be seen passing by.

for ssDNA

- Wash 10 $\mu$ l bead stock solution in TE-buffer (Dilute in 50 $\mu$ l TE and extract beads from the solution by holding a permanent magnet in proximity of Eppendorf tube, repeat 2-3x)
- Wash with 0.05% Tween
- Wash one more time in TE
- Incubate with 1 $\mu$ l dsDNA for 30min (dsDNA stock solution (see app.C) diluted 1:25000 - 1:30000 in TE)
- Incubate with 0.1M NaOH for 60min
- Wash carefully in TE (use big tips)
- Incubate with 10 $\mu$ l bio-BSA (10mg/ml) for 15min
- Add 1ml TE<sup>+</sup>

The washed magnetic beads (in TE<sup>+</sup>) are transferred to one of the syringes. For DNA incubation the valve of the corresponding syringe is opened for  $\sim$ 10min (dismount magnet head!) and afterwards the channel is flushed with TE-buffer for  $\sim$ 10min. Magnets are installed after no more beads can be seen passing by.

**RecA Solutions:** RecA stock solution (2mg/l), supplied in 0.1mM EDTA, 10mM Tris-HCl 7.5pH, 1mM DTT and 50% glycerol is provided by New England Biolabs<sup>®</sup> Inc.

## B. Appendix

- Mix 50 $\mu$ l of RecA stock solution with 950 $\mu$ l degased RecA binding buffer (corresponds to 2.6 $\mu$ M RecA solution)
- Add 1 $\mu$ l ATP $\gamma$ -s (100 $\mu$ M)
- Filter (0.22  $\mu$ m Millipore<sup>TM</sup> Millex<sup>®</sup> GV filter, PVDF membrane)

The filtered RecA solution is filled into a syringe connected with the magnetic bead or the adjacent channel (depending on the assay). For RecA assembly the valve is opened until full filament formation is achieved and subsequently flushed out with interaction buffer. RecA on ssDNA tend to disassemble. Therefore, for experiments where interactions with ssDNA·RecA NPF are probed, a slight RecA background is added to the interaction buffer (1 $\mu$ l stock solution RecA + 1 $\mu$ l ATP- $\gamma$ -s (100mM) or 1 $\mu$ ATP (100mM) in 3ml interaction buffer).

## C. Appendix

Procedures for the biological constructs:

- 7kb single strandable DNA for magnetic tweezers
- 12kb single strandable DNA for magnetic tweezers
- 48kb for optical tweezers
- 20kb single strandable DNA for optical tweezers
- heterologous 10kb for magnetic tweezers
- homologous 10kb for magnetic tweezers

### 7 kb ssDNA magnetic tweezers (experiment Y07005)

7329 kb PCR

Template: lamda DNA

Primers ordered at Biologio

199 5' DIG AACTCAGCTCACCGTCGAACA

68 5' BIO GACGCAGGGGACCTGCAG

PCR mix: 10  $\mu$ l HerculII buf (5x, Stratagene), 1  $\mu$ l primer 199 (10  $\mu$ M), 1  $\mu$ l primer 68 (10  $\mu$ M), 1  $\mu$ l dNTP's (10 mM, Promega), 2  $\mu$ l lambda DNA (10 ng/ $\mu$ l, Promega), 0,5  $\mu$ l Herc II fusion (Stratagene), 34,5  $\mu$ l MQ

PCR program: step 1 98°C 2:30, step 2 94°C 0:40, step 3 58°C 0:30, step 4 72°C 7:00, repeat step 2 to 4 29 times, step 5 72°C 8:00, step 6 20°C 0:30

PCR digoxigenin handle

PCR fragment (1238 bp)

PCR template pbluescriptIIISK+

Forward primer 5'GACCGAGATAGGGTTGAGTG 3' , reverse primer 5' CAGGGTCGGAACAGGAGAGC 3'.

The PCR reactions are performed with a taq polymerase (PCR core system I, Promega). Standard PCR reactions are performed, except 2  $\mu$ l of digoxigenin-11-2'-deoxy-uridine-5'- triphosphate (dig-dUTP, Roche) is added.

Both PCR products are purified with nucleospin extract II kit (Machery Nagel)

Cut both fragments with PspOMI (20 U/ $\mu$ l, NEB)

7329 bp fragment x PspOMI, fragment will lose 5' dig label  $\rightarrow$  7279 bp

Dig handle x PspOMI, 2 fragments after digestion 545-693 bp

Purify digestions with nucleospin extract II kit (Machery Nagel)

Ligate 7279 bp fragment (PspOMI overhang) with dig handle fragments (PspOMI overhang)

Ligation is performed with T4 DNA ligase (NEB)

Handles are added in 10 molar excess

Overnight ligation at 16°C

To purify the construct the ligation will be phenol extracted and ethanol precipitated. Phenol extraction is

## C. Appendix

done with the phase lock tubes (VWR) Ethanol precipitation is done according to Maniatis (2 1/2 V of 100% EtOH, and 1/10 V of 3M NaAc) Overnight precipitation -20°C. Pellet is dissolved in TE and ethanol is added to prevent nicking up to a final concentration of 1%.

### 12 kb ssDNA magnetic tweezers (experiment S1003, labjournal XII, S. Hage)

11940 kb PCR

Template: lamda DNA

Primers ordered at Biolegio

785 5' BIO CTCATGCTCACAGTCTGAGCGGTTCAACAGG

786 5' AACGCTTCACTCGAGGCGTTTTTCGTTATGTATAAATAAGGAGCACACC

PCR mix; 10  $\mu$ l Hercll buf (5x, Stratagene), 1  $\mu$ l primer 785 (10  $\mu$ M), 1  $\mu$ l primer 786 (10  $\mu$ M), 2  $\mu$ l dNTP's (10 mM, Promega), 1  $\mu$ l lambda DNA (50 ng/ $\mu$ l, Promega), 1  $\mu$ l Herc II fusion (Stratagene), 34  $\mu$ l MQ

PCR program: step 1 98°C 2:30, step 2 94°C 0:40, step 3 62°C 0:30, step 4 68°C 6:00, repeat step 2 to 4 9 times, step 5 94°C 0:40, step 6 62°C 0:30, step 7 68°C 6:00 + 0:10/ cycli, repeat step 5 to 7 19 times, step 8: 68°C 10:00, step 9 20°C 0:30

PCR digoxigenin handle

PCR fragment (1238 bp)

PCR template pbluescriptlISK+

Forward primer 5'GACCGAGATAGGGTTGAGTG 3'

Reverse primer 5' CAGGGTCGGAACAGGAGAGC 3'

The PCR reactions are performed with a taq polymerase (PCR core system I, Promega). Standard PCR reactions are performed, except 2  $\mu$ l of digoxigenin-11-2'-deoxy-uridine-5'- triphosphate (dig-dUTP, Roche) is added.

Both PCR products are purified with nucleospin extract II kit (Machery Nagel)

Cut both fragments with XhoI (20 U/ $\mu$ l, NEB)

11940 bp fragment x XhoI  $\rightarrow$  11926 bp

Dig handle x XhoI, 2 fragments after digestion 554-684 bp

Purify digestions with nucleospin extract II kit (Machery Nagel)

Ligate 11926 bp fragment (XhoI overhang) with dig handle fragments (XhoI overhang), Ligation is performed with T4 DNA ligase (NEB), Handles are added in 10 molar excess, Overnight ligation at 16°C.

To purify the construct the ligation will be phenol extracted and ethanol precipitated. Phenol extraction is done with the phase lock tubes (VWR) Ethanol precipitation is done according to Maniatis (2 1/2 V of 100% EtOH, and 1/10 V of 3M NaAc) Overnight precipitation -20°C. Pellet is dissolved in TE and ethanol is added to prevent nicking up to a final concentration of 1%.

## C. Appendix

### **Lambda (48kb) optical tweezers (experiment S1003, labjournal XII, S. Hage)**

35  $\mu$ l lambda DNA (645 ng/ $\mu$ l, Promega)

10 min at 65°C

On ice

Add 4  $\mu$ l bio-dCTP (0,4 mM, Invitrogen), 4  $\mu$ l bio-dATP (0,4 mM, Invitrogen), 0,5  $\mu$ l dGTP (10mM, Promega), 0,5  $\mu$ l dTTP (10mM, Promega), 4  $\mu$ l Klenow (-exo 5U/ $\mu$ l, NEB) 7  $\mu$ l Neb2 buf (10x, NEB), 18  $\mu$ l MQ, Incubate 2 h at 37°C

To purify the construct the ligation will be phenol extracted and ethanol precipitated. Phenol extraction is done with the phase lock tubes (VWR) Ethanol precipitation is done according to Maniatis (2 1/2 V of 100% EtOH, and 1/10 V of 3M NaAc) Overnight precipitation -20°C

Pellet is dissolved in TE and ethanol is added to prevent nicking up to a final concentration of 1%.

### **20 kb molecule optical tweezers (experiment S1003, labjournal XII, S. Hage)**

One of the strands is on both sides biotinylated

Molecule can be overstretched

20093 kb PCR

Template: lambda DNA

Primers ordered at Biologio

751 5' BIO CGTGCGAACTCTAGATGAATTTCTGAAAGAGTTACCCCTCTAAGTAATGAGG

755 5' BIO TCTGGAATTGGCAGAAGAAAACGTGCGATGGCAGCCAAAATTTGTGGCGG

T in primer 755 = biotin label

PCR mix; 10  $\mu$ l HerclI buf (5x, Stratagene), 5  $\mu$ l primer 751 (10  $\mu$ M), 5  $\mu$ l primer 755 (10  $\mu$ M), 2  $\mu$ l dNTP's (10 mM, Promega), 1  $\mu$ l lambda DNA (50 ng/ $\mu$ l, Promega), 1  $\mu$ l Herc II fusion (Stratagene), 2,5  $\mu$ l DMSO (Stratagene), 23,5  $\mu$ l MQ

PCR program: step 1 98°C 2:30, step 2 94°C 0:40, step 3 58°C 0:30, step 4 68°C 10:00, repeat step 2 to 4 9 times, step 5 94°C 0:40, step 6 58°C 0:30, step 7 68°C 10:00 + 0:10/ cycli, repeat step 5 to 7 19 times, step 8: 68°C 10:00, step 9 20°C 0:30

PCR product is purified with nucleospin extract II kit (Machery Nagel)

Fragment is digested with XbaI (20 U/ $\mu$ l, NEB), 1h 37C - fragment length after digestion 20083 bp

Fragment is purified with a G25 column (GE Healthcare)

Use fragment in Klenow fill-in reaction

Mixture 80  $\mu$ l DNA, 4  $\mu$ l Klenow (-exo 5 U/ $\mu$ l, NEB), 0,2  $\mu$ l dGTP (10 mM, Promega), 2  $\mu$ l bio-dUTP (1 nmol/ $\mu$ l, Roche), 5  $\mu$ l bio-dATP (0,4 mM Invitrogen), 5  $\mu$ l bio-dCTP (0,4mM Invitrogen) 11  $\mu$ l NEB2 buffer (NEB), 2,8  $\mu$ l MQ

Incubation 1 h 37°C

Heat inactivation 20 min 75°C

To purify the construct the ligation will be phenol extracted and ethanol precipitated. Phenol extraction is done with the phase lock tubes (VWR) Ethanol precipitation is done according to Maniatis (2 1/2 V of 100%

## C. Appendix

EtOH, and 1/10 V of 3M NaAc) Overnight precipitation -20°C

Pellet is dissolved in TE and ethanol is added to prevent nicking up to a final concentration of 1%.

### **10 kb heterolog magnetic tweezers construct (experiment S1003, labjournal XII, S. Hage)**

Fresh miniprep isolation (Quikpure kit, Machery Nagel) of plasmid pBlue1,2,4+ psfVI (collection BN no: GL003)

Cut plasmid with XbaI, SacI → 1954 - 10162 Gel extraction of 10162 bp fragment with nucleospin extract II kit (machery Nagel)

Digoxigenin ends:

PCR fragment (1238 bp)

PCR template pbluescriptIISK+

Forward primer 5'GACCGAGATAGGGTTGAGTG 3'

Reverse primer 5' CAGGGTCGGAACAGGAGAGC 3'

The PCR reactions are performed with a taq polymerase (PCR core system I, Promega). Standard PCR reactions are performed, except 2 µl of digoxigenin-11-2'-deoxy-uridine-5'- triphosphate (dig-dUTP, Roche) is added. PCR fragment is digested with SacI → 645 - 593 bp

Biotinylated:

PCR fragment (1238 bp)

PCR template pbluescriptIISK+

Forward primer 5'GACCGAGATAGGGTTGAGTG 3'

Reverse primer 5' CAGGGTCGGAACAGGAGAGC 3'

The PCR reactions are performed with a taq polymerase (PCR core system I, Promega). Standard PCR reactions are performed, except 2 µl of Biotin-16-2'-deoxy-uridine-5'- triphosphate (bio-dUTP 50 nmol, Roche) is added. PCR fragment is digested with XbaI → 617 - 621 bp

Both digestions of the handles are purified with the nucleospin extraction kit (machery Nagel)

Ligate 10162 bp fragment (XbaI, SacI overhang) with dig handle fragments (SacI overhang) and bio handle fragments (XbaI overhang). Ligation is performed with T4 DNA ligase (NEB) Handles are added in 10 molair excess Overnight ligation at 16°C.

To purify the construct the ligation will be phenol extracted and ethanol precipitated. Phenol extraction is done with the phase lock tubes (VWR) Ethanol precipitation is done according to Maniatis (2 1/2 V of 100% EtOH, and 1/10 V of 3M NaAc) Overnight precipitation -20C. Pellet is dissolved in TE and ethanol is added to prevent nicking up to a final concentration of 1%.

### **10 kb homolog magnetic tweezers construct (experiment S1003, labjournal XII, S. Hage)**

Fresh miniprep isolation (Quikpure kit, Machery Nagel) of plasmid pSFVIIlambda (collection BN no: GL120)

Cut plasmid with XbaI, BamHI, AflII 475 - 287 - 10118 bp

Purify digestion with nucleospin extract II kit (machery Nagel)

Digoxigenin ends: PCR fragment (1238 bp)

PCR template pbluescriptIISK+

Forward primer 5'GACCGAGATAGGGTTGAGTG 3'

Reverse primer 5' CAGGGTCGGAACAGGAGAGC 3'

## D. Appendix

The PCR reactions are performed with a taq polymerase (PCR core system I, Promega). Standard PCR reactions are performed, except 2  $\mu$ l of digoxigenin-11-2'-deoxy-uridine-5'- triphosphate (dig-dUTP, Roche) is added. PCR fragment is digested with BamHI 605  $\ddot{U}$  633 bp

Biotinylated:

PCR fragment (1238 bp)

PCR template pbluescriptIISK+

Forward primer 5'GACCGAGATAGGGTTGAGTG 3'

Reverse primer 5' CAGGGTCGGAACAGGAGAGC 3'

The PCR reactions are performed with a taq polymerase (PCR core system I, Promega). Standard PCR reactions are performed, except 2  $\mu$ l of Biotin-16-2'-deoxy-uridine-5'- triphosphate (bio-dUTP 50 nmol, Roche) is added. PCR fragment is digested with Xbal 617  $\ddot{U}$  621 bp

Both digestions of the handles are purified with the nucleospin extraction kit (machery Nagel)

Ligate 10118 bp fragment (Xbal, BamHI overhang) with dig handle fragments (BamHI overhang) and bio handle fragments (Xbal overhang). Ligation is performed with T4 DNA ligase (NEB), Handles are added in 10 molair excess, Overnight ligation at 16°C.

To purify the construct the ligation will be phenol extracted and ethanol precipitated. Phenol extraction is done with the phase lock tubes (VWR) Ethanol precipitation is done according to Maniatis (2 1/2 V of 100% EtOH, and 1/10 V of 3M NaAc) Overnight precipitation -20C.Pellet is dissolved in TE and ethanol is added to prevent nicking up to a final concentration of 1%.

## D. Appendix

### Interatomar distance of the atoms constituting the DNA backbone between two bases

The chain of molecules between the carbon atom at the 5'-deoxsyribose position of one base to the carbon atom at the 3'-deoxsyribose position is C-C-O-P-O-C. The binding angle between the atoms of the chain is approximated with 120°, resulting in a base-to-base distance of  $\sim 6.19\text{\AA}$ .

Table 3: Atom radii and resulting interatomar binding distances

Atom	Radius [ $\text{\AA}$ ]	Bond	Length [ $\text{\AA}$ ]
C	0.77	C-C	1.54
O	0.66	C-O	1.43
p	1.10	P-O	1.76



**Philosophisch-Naturwissenschaftliche Fakultät  
der Universität Basel  
Dekanat**

**Erklärung zur wissenschaftlichen Redlichkeit**  
(beinhaltet Erklärung zu Plagiat und Betrug)

(bitte ankreuzen)

- Bachelorarbeit  
 Masterarbeit

Titel der Arbeit (Druckschrift):

Description in the certificate: Single molecule biophysics of homologous recombination

Title of the thesis: The mechanics of recombination disentangled by dual molecule measurements

Name, Vorname (Druckschrift): Zweifel, Ludovit Pavel

Matrikelnummer: 04-052-288

Hiermit erkläre ich, dass mir bei der Abfassung dieser Arbeit nur die darin angegebene Hilfe zuteil wurde und dass ich sie nur mit den in der Arbeit angegebenen Hilfsmitteln verfasst habe.

Ich habe sämtliche verwendeten Quellen erwähnt und gemäss anerkannten wissenschaftlichen Regeln zitiert.

Diese Erklärung wird ergänzt durch eine separat abgeschlossene Vereinbarung bezüglich der Veröffentlichung oder öffentlichen Zugänglichkeit dieser Arbeit.

ja  nein

Ort, Datum: Basel, 29. Mai 2011

Unterschrift: 

Dieses Blatt ist in die Bachelor-, resp. Masterarbeit einzufügen.